BASE PRESSURE COEFFICIENTS OBTAINED FROM THE X-15 AIRPLANE FOR MACH NUMBERS UP TO 6

by Edwin J. Saltzman

Flight Research Center
Edwards, Calif.

BASE PRESSURE COEFFICIENTS OBTAINED

FROM THE X-15 AIRPLANE FOR MACH NUMBERS UP TO 6

By Edwin J. Saltzman

Flight Research Center
Edwards, Calif.

NATIONAL AERONAUTICS AND SPACE ADMINISTRATION

BASE PRESSURE COEFFICIENTS OBTAINED

FROM THE X-15 AIRPLANE FOR MACH NUMBERS UP TO 6

By Edwin J. Saltzman
Flight Research Center

SUMMARY

Power-off and power-on base pressures measured on the X-15 airplane are compared with wind-tunnel data, semiempirical estimates, and theory. The results indicate that the supersonic base pressure characteristics of the upper vertical fin are relatively insensitive to span position and are closely predicted by two-dimensional theory for thin boundary layers. Flight power-off base pressure coefficients for the fuselage, side fairing, and vertical fin are higher (higher negative values) than obtained on X-15 wind-tunnel models throughout a comparable speed range. At a Mach number of 3, the flight values are about 15 percent higher.

For most supersonic speeds, the effect of the exhaust jet on the base pressure is about the same along the vertical fin as at the fuselage flameshield; that is, the effect is about the same 5 jet radii from the edge of the jet as it is 1/5 radius from the jet.

INTRODUCTION

On many future aircraft and reentry configurations, smooth aerodynamic lines will be compromised in favor of stability and/or propulsion requirements. Such requirements can result in blunt trailing edges on stabilizing surfaces, or in a blunt center-body base remaining after engine shutdown or separation from a booster. Such abrupt changes in cross-sectional area add significantly to the drag of a vehicle, especially at the lower supersonic speeds. For this reason, the study of base pressure has received increasing emphasis during the past several years. Theoretical studies have been made and many scaled wind-tunnel-model base pressure experiments simulating unpowered flight have been conducted, such as the studies of references 1 to 4. More recently, the effects of jet-exhaust flow on model base pressures have been treated (refs. 5 to 9).

This paper presents full-scale results obtained from the various base elements of the X-15 research airplane. The X-15 has a relatively large base area, about one-sixth of the wing area, and is capable of a wide range of flight speeds. Thus, wind-tunnel, semiempirical, and theoretical results can be compared with full-scale flight results.

Preliminary base pressure coefficients from the first two X-15 flights in which base pressure data were recorded were reported in reference 10. These data, which ranged in Mach number from 1.1 to 3.2, were obtained while the X-15 was powered by the interim rocket engines which had a total thrust of about 16,000 pounds at burnout altitude. The airplane now has a larger power plant which develops about 58,000 pounds of thrust at burnout altitude. This thrust increase extends the Mach number range to 6 and, of course, has a significant effect on the base pressures during engine operation.

The base pressure data presented in this paper were obtained after the large power plant was installed. Power-off data are included for each major base element of the airplane and are compared to available wind-tunnel data and to results from some of the techniques of predicting base pressure. The base drag resulting from these base pressures was reported in reference 11. The effects of the rocket-engine exhaust on base pressure are also shown. Trailing-shock pressure ratios, calculated for a simplified model of the flow behind the X-15 during powered flight, are discussed in the appendix.

SYMBOLS

$C_{p,b}$ base pressure coefficient, $\dfrac{p_b - p}{q}$

c chord, in. or ft

d_f maximum diameter of fuselage or body, in.

d_j diameter of the jet at base station, in.

h trailing-edge thickness, in.

l distance forward of jet exit station, in.

M free-stream Mach number

M_e Mach number along boattail (external flow)

M_e' Mach number after expansion to base static pressure

M_j Mach number of exhaust jet at exit station

M_j' Mach number after expansion to base static pressure

N_{R_e} free-stream Reynolds number per foot, $\dfrac{\rho V}{\mu}$

p free-stream static pressure, lb/sq ft

p_b base static pressure, lb/sq ft

p_e static pressure on boattail surface ahead of base (external flow), lb/sq ft

p_j	static pressure at exhaust jet exit station, lb/sq ft
p_w	static pressure in wake, behind trailing shock, lb/sq ft
q	free-stream dynamic pressure, $0.7M^2p$, lb/sq ft
R	gas constant, ft^2/sec^2 °R
r_j	radius of jet at exhaust plane, in.
V	true airspeed, ft/sec
$\dot{w}$	air flow rate, lb/sec
$\dot{w}_j$	jet flow rate, lb/sec
X	mixing-length ratio
z	distance from orifice to edge of jet at exhaust plane, in.
β	boattail angle, deg
γ	ratio of specific heat for air
γ_j	ratio of specific heat for exhaust gas
Δ	estimated error
λ	nozzle half-angle, deg
μ	absolute viscosity, lb-sec/ft^2
ρ	air density, slugs/cu ft

AIRPLANE

The X-15 is a single-place, low-aspect-ratio monoplane designed for manned flight research up to Mach numbers near 6. A three-view drawing and a photograph of the airplane are shown in figures 1 and 2, respectively. Physical characteristics of the airplane are presented in table I.

The X-15 is carried to an altitude of about 45,000 feet by a modified B-52 bomber and is launched at a Mach number of approximately 0.8. For the flights reported herein, the X-15 was powered by the YLR99 rocket engine which develops about 58,000 pounds of thrust at full throttle. For the full-throttle condition, powered flight can be maintained for about 85 seconds, after which the airplane glides for 8 to 10 minutes before landing on the dry lake at Edwards, Calif.

A photograph of the airplane viewed directly from the rear is shown in figure 3, and a left rear view of the fuselage is shown in figure 4. It can be

seen that the base region formed by the closed speed brakes is open to the rear and does not have a base surface behind the speed-brake hinge line. The outline of the open speed brakes is shown by the dashed lines in figure 3. As indicated in the Introduction, the early flights of the X-15 were made with an interim power plant. The base configuration for those flights and for the data of reference 10 is shown in figure 5.

Rocket-engine characteristics and pertinent base and fuselage afterbody dimensions are presented in table II.

INSTRUMENTATION

The location of each orifice used to obtain base pressures is shown in figure 6. These orifices were connected to aneroid-type pressure cells mounted in a standard NASA 12-cell photorecording manometer. Maximum limits for lag in the pressure-sensing system were evaluated by observing the elapsed time for a pressure change to be recorded after the rocket engine was ignited or shut down. The lag in the system was found to be negligible for most of the data in this paper (less than 1/2 second); the maximum lag is estimated to be less than 1 second.

Radar tracking information was used in conjunction with radiosonde balloon data to obtain free-stream velocity, altitude, Mach number, and dynamic pressure. (See ref. 12 for details of this procedure.)

Other flight parameters pertinent to this study were measured on standard NASA flight data-recording instruments, and all records were synchronized by a common timer.

ERROR AND RELIABILITY

The primary sources of error affecting the accuracy of power-off base pressure coefficients obtained during this investigation are true airspeed V, base pressure p_b, and free-stream static pressure p. The resulting errors in base pressure coefficient attributable to the maximum estimated deviations for these sources of error are listed in the following table:

M	$\Delta c_{p,b}$ resulting from -			Limit $\Delta c_{p,b}$	Limit, percent $\dfrac{\Delta c_{p,b}}{c_{p,b}}$	Faired, percent $\dfrac{\Delta c_{p,b}}{c_{p,b}}$
	ΔV	Δp_b	Δp			
1.5	±0.014	±0.012	±0.012	±0.038	±11	±3
3.0	±0.005	±0.009	±0.002	±0.016	±13	±4
6.0	±0.001	±0.006	±0.001	±0.008	±28	±8

4

p_j	static pressure at exhaust jet exit station, lb/sq ft
p_w	static pressure in wake, behind trailing shock, lb/sq ft
q	free-stream dynamic pressure, $0.7M^2p$, lb/sq ft
R	gas constant, ft^2/sec^2 °R
r_j	radius of jet at exhaust plane, in.
V	true airspeed, ft/sec
$\dot{w}$	air flow rate, lb/sec
$\dot{w}_j$	jet flow rate, lb/sec
X	mixing-length ratio
z	distance from orifice to edge of jet at exhaust plane, in.
β	boattail angle, deg
γ	ratio of specific heat for air
γ_j	ratio of specific heat for exhaust gas
Δ	estimated error
λ	nozzle half-angle, deg
μ	absolute viscosity, lb-sec/ft^2
ρ	air density, slugs/cu ft

AIRPLANE

The X-15 is a single-place, low-aspect-ratio monoplane designed for manned flight research up to Mach numbers near 6. A three-view drawing and a photograph of the airplane are shown in figures 1 and 2, respectively. Physical characteristics of the airplane are presented in table I.

The X-15 is carried to an altitude of about 45,000 feet by a modified B-52 bomber and is launched at a Mach number of approximately 0.8. For the flights reported herein, the X-15 was powered by the YLR99 rocket engine which develops about 58,000 pounds of thrust at full throttle. For the full-throttle condition, powered flight can be maintained for about 85 seconds, after which the airplane glides for 8 to 10 minutes before landing on the dry lake at Edwards, Calif.

A photograph of the airplane viewed directly from the rear is shown in figure 3, and a left rear view of the fuselage is shown in figure 4. It can be

Because the sign and magnitude of these individual source errors can vary at random, within the limits shown, they tend to cancel one another. Thus, the resultant dispersion of the main body of data points about the true value is less than the limit $\Delta C_{p,b}$ indicated. For figures which are derived from fairings through the raw values of $C_{p,b}$ plotted against M (fig. 7), the net error is estimated to be within the values shown in the last column.

Power-on data would usually have somewhat larger errors because of the larger gradients in velocity and pressure as the airplane accelerates to higher altitude.

A fuel vent line on the interim configuration that is not on the configuration of this study can be seen by comparing figures 3 and 5. The line was added to the interim configuration of reference 10 after the pressure orifices were installed. It is believed, therefore, that the configuration of the present study, without the vent line, provides the most reliable data for the adjacent side fairing and fuselage base elements because of probable interference effects from the vent line. In addition, it should be noted that most of the power-off data presented herein, except for figure 7(g), were obtained from 6 flights and the power-on data from 11 flights. The results of reference 10 represent only two flights; thus, the present study is considered to be more comprehensive.

TEST CONDITIONS

Base pressure data were obtained over a Mach number range from about 0.8 to 6.0. Unit Reynolds number (per foot of surface length) varied from about 7×10^5 to 2.6×10^6. The X-15 has many protuberances, gaps, and notches scattered over its surfaces, and in some areas of the fuselage and vertical fins the skin is wavy. Hence, except for local areas of laminar flow, primarily on the wings, horizontal tail, and lower fin, the flow is turbulent for the maneuvers considered in this study. Certainly, turbulence occurred ahead of the base regions in every case considered for the present tests.

Sideslip was held to within ±1° during the tests, and angle of attack varied between -2° and 12°. The jettisonable portion of the lower fin was attached for all of the flights included herein. Other conditions, such as speed-brake position or engine operation, that are pertinent to the data are noted in the figures.

POWER-OFF RESULTS

Basic Data

Variables usually believed to affect base pressure are Mach number, the ratio of jet exhaust to free-stream static pressure, Reynolds number, and angle of attack. Analysis of the data of this paper reveals a consistent relationship between base pressure and the first two variables, but there is no apparent

5

variation of base pressure coefficient with respect to Reynolds number or angle of attack for the range of the conditions considered. This lack of variation is not unexpected because, as noted previously, the flow over the various surfaces becomes turbulent before it reaches the base regions. Other investigators (refs. 1 to 3) have shown, too, that Reynolds number effects on base pressure are relatively small for turbulent flow; thus, most of the data in this paper are plotted without regard to Reynolds number. Similarly, on the basis of the present investigation and the results of references 1, 2, and 10, the data are plotted without regard to angle of attack.

The basic data for each of the eight major base elements are shown in figures 7(a) to 7(h) in which the base pressure coefficient is plotted against free-stream Mach number. For most of the base elements (figs. 7(a) to 7(d), and 7(h)), speed-brake deflection causes an increase in base pressure coefficient[1] (results in higher base drag) at supersonic Mach numbers below 2 or 2.5. At higher Mach numbers, deflection of the speed brakes has little effect on base pressure except for the side fairing (fig. 7(f)), where deflection reduces the pressure coefficient by about one-half. As would be expected because of its relative location, the base pressure of the wing trailing edge is unaffected by speed-brake deflection or engine operation (fig. 7(g)). Thus, this location may be, after careful calibration, a reliable indirect source of free-stream static pressure. Further study would be necessary to establish the consistency of the pressure coefficients from this orifice, however.

Data from figures 7(a) to 7(d), which represent the base pressures obtained from the movable and stationary portions of the upper vertical fin, are replotted in figure 8 to reveal possible span-position effects on the X-15 fin. Reference 2 indicates that the base pressure of thin wings is relatively insensitive to span position at low supersonic speeds. Figure 8 shows that, with the possible exception of the data for $M = 1.5$, there is no significant or orderly variation of base pressure coefficient with span position at supersonic speeds, even though the X-15 fuselage terminates within 20 inches of the fin root base.

Comparison of Flight Data With Wind-Tunnel Tests of Blunt-Trailing-Edge Wings

In the study of reference 10, it was found that the base pressure data of the upper vertical fin compared well with small-scale blunt-trailing-edge wing data obtained from the wind-tunnel tests of reference 2. Near the end of the present study, an additional pressure orifice was added at the wing trailing edge to permit comparisons between the vertical-fin data and data from a full-scale blunt-trailing-edge wing. This comparison is shown in figure 9. As can be seen, the trend of the data is similar, but the values of the fin base pressure coefficients are consistently higher than are those for the wing (each based on free-stream conditions).

---

[1]An increase in base pressure coefficient as used herein refers to an increase in negative pressure coefficient (in an absolute sense), which results in increased base drag.

Reference 2 shows that, for a given Mach number, the curve of $\frac{p_b}{p}$ plotted against $\frac{c}{h\left(N_{R_e}\right)^{1/5}}$ is satisfactory for correlating turbulent-flow base pressure characteristics of blunt-trailing-edge wings having base thicknesses from 5 percent to 10 percent of the chord length and boattail angles ranging from positive to negative. Data presented in the form of these parameters are shown in figure 10. Experimental results are shown for the X-15 upper vertical fin and wing bases as well as for the small-scale wing tests of reference 2. Also included are theoretical values (ref. 4)[1] of base pressure ratio for thin turbulent boundary layers. For Mach numbers of 1.5 to 2.0 where the flow ahead of the X-15 wing and fin is less subject to the forebody (than at higher Mach numbers) and where there is little influence on wing base pressure from varied forebodies (ref. 2), the following observation is made: The wing and fin data (considered together as establishing a trend) agree with the wind-tunnel results of reference 2 in approaching the theoretical values for thin boundary layers as $\frac{c}{h}$ is reduced. At $M = 3.1$ the flight value for the fin (which has a low value of $\frac{c}{h}$) agrees well with the wind-tunnel results and theory. The wing value of $\frac{p_b}{p}$, however, falls significantly below the wind-tunnel data. This disagreement for the wing data at $M = 3.1$ may result from expansion waves originating over the side fairing and subsequently affecting the flow ahead of the wing.

Comparison of Flight Data With Wind-Tunnel Tests of X-15 Models

The base pressure coefficients from tests on several X-15 wind-tunnel models are compared in figure 11 with the faired values of the full-scale flight data of figure 7. The models represented by references 11, 13, and 14 are nearly exact models of the full-scale airplane, whereas the model of reference 15 is of an earlier configuration of the X-15 with a different side fairing and vertical-tail shape.

Figure 11 shows somewhat lower base pressure coefficients for the model data than for full-scale flight. At $M = 3$, for example, the base pressure coefficients, or base drag, are about 15 percent lower for the models than for the airplane. This disagreement is considered conclusive, inasmuch as the data were obtained from four separate tests in three different wind tunnels and from

---

[1]The theory of reference 4 as used herein is applicable only at the lowest values of $\frac{c}{h}$ where the boundary layer is thin relative to the base thickness. Because Reynolds number for turbulent flow has little influence on base pressure, this theory is likewise applicable only at the lowest values of $\frac{c}{h\left(N_{R_e}\right)^{1/5}}$. The theory is based on the concepts of interaction between the dissipative shear flow and the adjacent free stream and on the conservation of mass in the wake.

six flights. This disagreement did not constitute a performance problem for the X-15, which has a maximum thrust-weight ratio of about 3.5 and excess energy for its fixed range of operation. However, such a discrepancy between expected and actual base pressures would have serious consequences for a long-range supersonic-cruise aircraft with a lower thrust-to-weight ratio.

<div align="center">

Comparison of Flight Data With Theory
and Semiempirical Methods

</div>

In figure 12, the average base pressure coefficient measured on the upper vertical fin during power-off flight is compared with the two-dimensional theory of Korst for thin boundary layers (ref. 4) and the two-dimensional semiempirical estimate of Love (ref. 1). As in figure 10, the theory agrees well with the full-scale fin data. The semiempirical estimate of Love predicts the trend of pressure coefficient with Mach number but underestimates the absolute value. These estimates are based on an analogy between the trailing-shock pressure rise and the peak pressure rise associated with the separation of a turbulent boundary layer on a flat plate caused by a forward facing step. Equation (6) of reference 16 was used to define the peak pressure rise for Mach numbers less than 4, and empirical results from reference 17 were used at the higher Mach numbers.

Also shown in figure 12 are the curves for zero base pressure and the hypersonic approximation $-\frac{1}{M^2}$. At Mach numbers between 4 and 5, the flight data approach the limiting curve ($p_b = 0$), and near $M = 6$ the value $-\frac{1}{M^2}$ results in reasonable agreement with flight.

In figure 13, full-scale-flight base pressure coefficients obtained from the fuselage are compared with adaptations of semiempirical estimates from reference 1 for a body of revolution. The cylindrical-body estimates are considerably lower than the full-scale flight values for Mach numbers below 4. When conditions ahead of the base are chosen that account for the expansion over the fuselage boattail, the estimated values are much closer to the flight data for these Mach numbers. An attempt was made to estimate the combined effect of the boattail and the vertical fin on the fuselage base pressure coefficient. As can be seen, the result, which is representative of an orifice behind the expansion waves of the fin base, greatly overestimates the base pressure coefficients obtained in flight and approaches the limiting condition for a vacuum. The hypersonic approximation agrees well with the flight data at the higher Mach numbers.

<div align="center">

POWER-ON RESULTS

</div>

As was shown in figure 7, for orifices near the rear of the airplane, the base pressure coefficients obtained from power-off flight are repeatable as a function of Mach number. When the rocket engine is operating, however, these base pressure coefficients are no longer a simple function of free-stream Mach number. The increase in scatter caused by the exhaust jet can be seen by

8

comparing the power-on fuselage flameshield data of figure 14 with the power-off data of figure 7(e). The expected reduction of the base pressure coefficients with rocket operation is also readily apparent in figure 14.

A greater degree of order with the power-on data can be achieved by introducing a variable involving the rocket engine. A commonly used parameter (refs. 6, 7, and 18) is the ratio of the static pressure at the jet exit plane to free-stream static pressure $\frac{p_j}{p}$. The relationship of base pressure coefficient to this ratio is shown for several Mach numbers in figure 15. At the lowest Mach number, 1.5, base pressure coefficient is extremely sensitive to $\frac{p_j}{p}$. At higher Mach numbers (M = 3, for example), the base pressure coefficient is much less sensitive; that is, the slope of $C_{p,b}$ with respect to $\frac{p_j}{p}$ becomes progressively less as Mach number is increased.

Static pressure at the jet exit station p_j is, of course, directly related to rocket-chamber pressure. Similarly, the mass flow of propellant through the nozzle is related to chamber pressure. Consequently, the ratio of the weight of propellant flowing per unit of time to that of free-stream air flowing through a given area per unit of time $\frac{\dot{w}_j}{\dot{w}}$ should be expected to have a relationship to base pressure similar to that for $\frac{p_j}{p}$. Figure 16 shows the calculated relationship of these two ratios for several Mach numbers. The slopes of $C_{p,b}$ as related to both of the flow parameters are plotted in figure 17 as a function of free-stream Mach number. Although these data do not explain the phenomena in the flow field around the base region, they do provide a greater degree of order for power-on data than was shown in figure 14.

The effect of rocket operation on the pressures over other base elements farther from the jet flow should be considered. Of particular interest are orifices 1 to 4 on the vertical fin (fig. 6), because of their progressively increasing distances from the jet flow. Since the slope of $C_{p,b}$ with respect to $\frac{p_j}{p}$ for a given Mach number may be considered a relative measure of jet influence, that is, a (jet) base pressure decay parameter, data from these orifices are compared to data from the flameshield orifice (5) in figure 18. Although the influence of the jet might be expected to be related to some function of the reciprocal of distance from the jet, the slopes shown in figure 18 are seemingly independent of location for the distances involved, even though the distances vary from about 1/5 of the jet radius to 5 jet radii. Apparently, the "dead air" region that results from separation of the flow passing by the base is an effective channel for equalizing the pressure throughout the base.

The slope of $C_{p,b}$ with respect to $\frac{p_j}{p}$ from the X-15 is compared in figure 19 with wind-tunnel results (models with base annulus and simulated jet)

from references 19 and 20 and with predicted values from reference 21. As can be seen, the wind-tunnel results and the predicted values are considerably higher than the X-15 data at the lowest comparable Mach numbers. At intermediate Mach numbers, between 2.5 and 3.0, the disagreement is significantly smaller. The data from reference 20 have been adjusted to a nozzle half-angle of 20° by a coefficient derived from the data of reference 19. The resulting slopes (triangles) are somewhat lower than the flight values at the highest Mach numbers, but the trends are similar. The results from references 19 and 20 were for a boattail angle of 0°. The predictions of reference 21 accounted for boattail angle, but no attempt was made to account for jet exit Mach number. The data of references 19 to 21 did not include the effects of fins, which may be a major cause for the disagreement with the X-15 results.

CONCLUSIONS

Comparison of power-off and power-on base pressures measured on the X-15 airplane with wind-tunnel results, semiempirical estimates, and theory showed that:

1. Supersonic power-off base pressures along the upper vertical fin were relatively insensitive to span position and were closely predicted by two-dimensional theory for thin boundary layers.

2. Flight power-off base pressure coefficients for the fuselage, side fairing, and vertical fin were higher (higher negative values) than obtained on X-15 wind-tunnel models throughout a comparable speed range. At a Mach number of 3, the flight values were about 15 percent higher.

3. For most supersonic speeds, the effect of the exhaust jet on base pressure was about the same along the vertical fin as at the fuselage flameshield; that is, the effect was about the same 5 jet radii from the jet as it was 1/5 radius from the jet.

Flight Research Center,
    National Aeronautics and Space Administration,
        Edwards, Calif., May 7, 1964.

10

APPENDIX

TRAILING-SHOCK PRESSURE-RATIO CALCULATIONS

In many reports pertaining to base pressure, the trailing-shock pressure ratio $\dfrac{p_w}{p_b}$ is considered an important part of the flow model for treating base flow problems. Thus, a brief study was made of the trailing-shock pressure ratio for the X-15 fuselage base during rocket-engine operation, using the method presented in appendix B of reference 7. A model of the flow field used is shown in the following sketch:

Centerline of rocket nozzle
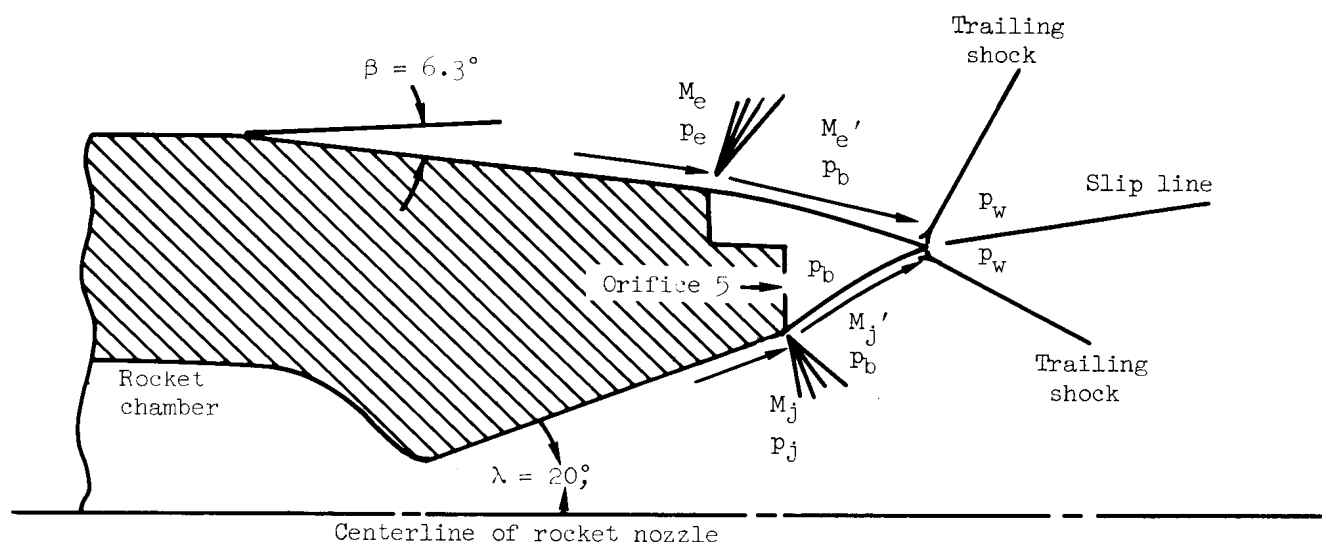
The flow of both the internal and external streams was considered to expand to the measured base pressure immediately upon reaching the base station. The Prandtl-Meyer turning angle for the jetstream was interpolated from figure 48 of reference 8 for a specific-heat ratio of 1.23, a commonly used value for a liquid-oxygen—ammonia propellant combination. The curvature of the internal stream was then estimated by cross-plotting data from reference 8, and the external-flow curvature was approximated through interpolation and cross-plotting the characteristics solutions presented in reference 3.

It was then required, at the point of intersection of the internal and external streams, that the resulting trailing shocks deflect the streams so that behind the shock waves their flow was parallel and the static pressure equal. For the external flow ($\gamma = 1.4$), references 22 and 23 were used to obtain conical and plane shock relationships. For the internal jet flow ($\gamma = 1.23$), equation (151) of reference 23 was employed. The approximation obtained from the several terms in this equation was adjusted by a coefficient consisting of the ratio of the exact solution with respect to the approximate solution for $\gamma = 1.4$. The effects of the boundary-layer and total-temperature profiles were disregarded

in these calculations. The trailing shock for the external flow was the result of calculated upstream Mach numbers as low as 1.71, so both plane and conical shock waves were considered. For the internal or jet flow, the calculated Mach numbers ahead of the shock were always above 3.9, thus only the plane shock was used.

Figure 20 shows the trailing-shock pressure ratios calculated for the X-15 flameshield, based upon the flow model in the preceding sketch, the experimental values of base pressure obtained from the flameshield orifice, and the coincident values of jet exit pressure, free-stream Mach number, and ambient pressure. Included are theoretical values of $\frac{p_w}{p_b}$ obtained by interpolation of figure 26 of reference 9. The theoretical values are the result of the limiting streamline analysis, also used in reference 7, which takes into account mixing along the boundaries of the internal and external flow while a constant mass is maintained within the base "dead air" region. The jet total-temperature effects have also been included. The interpolated theoretical values from reference 9 represent exhaust-gas properties and mixing-length ratios which do not duplicate the actual jet conditions. Adjustments have been made to these values, however, which provide trailing-shock pressure ratios which are based upon the physical properties of the actual jet. It is of interest to note that the simplified flow model used in the calculations of this appendix provides trailing-shock pressure ratios which agree closely with the theoretical values (accounting for the boundary-layer and total-temperature profiles) at the lower Mach numbers where the sensitivity of base pressure to jet flow is greatest. Although a detailed study including boundary layer and total-temperature-profile effects is beyond the scope of this paper, some readers may be interested in constructing a more realistic flow model such as was used in reference 9. An important contribution to such an effort would be the material of references 24 to 27.

REFERENCES

1. Love, Eugene S.: Base Pressure at Supersonic Speeds on Two-Dimensional Airfoils and on Bodies of Revolution With and Without Fins Having Turbulent Boundary Layers. NACA TN 3819, 1957. (Supersedes NACA RM L53C02.)

2. Chapman, Dean R., Wimbrow, William R., and Kester, Robert H.: Experimental Investigation of Base Pressure on Blunt-Trailing-Edge Wings at Supersonic Velocities. NACA Rep. 1109, 1952. (Supersedes NACA TN 2611.)

3. Chapman, Dean R.: An Analysis of Base Pressure at Supersonic Velocities and Comparison With Experiment. NACA Rep. 1051, 1951. (Supersedes NACA TN 2137.)

4. Korst, H. H.: A Theory for Base Pressures in Transonic and Supersonic Flow. Jour. App. Mech., vol. 23, no. 4, Dec. 1956, pp. 593-600.

5. Coletti, Donald E.: Measurements and Predictions of Flow Conditions on a Two-Dimensional Base Separating a Mach Number 3.36 Jet and a Mach Number 1.55 Outer Stream. NACA RM L54C08, 1954.

6. Cortright, Edgar M., Jr., and Kochendorfer, Fred D.: Jet Effects on Flow Over Afterbodies in Supersonic Stream. NACA RM E53H25, 1953.

7. Baughman, L. Eugene, and Kochendorfer, Fred D.: Jet Effects on Base Pressures of Conical Afterbodies at Mach 1.91 and 3.12. NACA RM E57E06, 1957.

8. Love, Eugene S., Grigsby, Carl E., Lee, Louise P., and Woodling, Mildred J.: Experimental and Theoretical Studies of Axisymmetric Free Jets. NASA TR R-6, 1959. (Supersedes NACA RM L54L31, RM L55J14, RM L56G18, and TN 4195.)

9. Beheim, Milton A., Klann, John L., and Yeager, Richard A.: Jet Effects on Annular Base Pressure and Temperature in a Supersonic Stream. NASA TR R-125, 1962.

10. Saltzman, Edwin J.: Preliminary Base Pressures Obtained From the X-15 Airplane at Mach Numbers From 1.1 to 3.2. NASA TN D-1056, 1961.

11. Hopkins, Edward J., Fetterman, David E., Jr., and Saltzman, Edwin J.: Comparison of Full-Scale Lift and Drag Characteristics of the X-15 Airplane With Wind-Tunnel Results and Theory. NASA TM X-713, 1962.

12. Larson, Terry J., and Webb, Lannie D.: Calibrations and Comparisons of Pressure-Type Airspeed-Altitude Systems of the X-15 Airplane From Subsonic to High Supersonic Speeds. NASA TN D-1724, 1963.

13. Franklin, Arthur E., and Lust, Robert M.: Investigation of the Aerodynamic Characteristics of a 0.067-Scale Model of the X-15 Airplane (Configuration 3) at Mach Numbers of 2.29, 2.98, and 4.65. NASA TM X-38, 1959.

14. Leupold, Mathias J., and Freeman, Elizabeth M.: A Second Series of Supersonic Force Tests on the Full-Span Model X-15 for North American Aviation Incorporated. WTR 200, Mass. Inst. of Tech. (Naval Supersonic Laboratory), Sept. 1958.

15. Franklin, Arthur E., and Silvers, H. Norman: Investigation of the Aerodynamic Characteristics of a 0.067-Scale Model of the X-15 Airplane (Configuration 2) at Mach Numbers of 2.29, 2.98, 3.96, and 4.65. NASA MEMO 4-27-59L, 1959.

16. Love, Eugene S.: Pressure Rise Associated With Shock-Induced Boundary-Layer Separation. NACA TN 3601, 1955.

17. Sterrett, James R., and Emery, James C.: Extension of Boundary-Layer-Separation Criteria to a Mach Number of 6.5 by Utilizing Flat Plates With Forward-Facing Steps. NASA TN D-618, 1960.

18. Cortright, Edgar M., Jr.: Some Aerodynamic Considerations of Nozzle-Afterbody Combinations. Aero. Eng. Rev., vol. 15, no. 9, Sept. 1956, pp. 59-65.

19. Bromm, August F., Jr., and O'Donnell, Robert M.: Investigation at Supersonic Speeds of the Effect of Jet Mach Number and Divergence Angle of the Nozzle Upon the Pressure of the Base Annulus of a Body of Revolution. NACA RM L54I16, 1954.

20. Charczenko, Nickolai, and Hayes, Clyde: Jet Effects at Supersonic Speeds on Base and Afterbody Pressures of a Missile Model Having Single and Multiple Jets. NASA TN D-2046, 1963.

21. Boren, T. C., and Hatalsky, William: Jet Effects Upon Base Drag. Gen. Dynamics/Pomona, 1960.

22. Dailey, C. L., and Wood, F. C.: Computation Curves for Compressible Fluid Problems. John Wiley & Sons, Inc., 1949.

23. Ames Research Staff: Equations, Tables, and Charts for Compressible Flow. NACA Rep. 1135, 1953. (Supersedes NACA TN 1428.)

24. Korst, H. H., Page, R. H., and Childs, M. E.: Compressible Two-Dimensional Jet Mixing at Constant Pressure. Tech. Note 392-1 (Contract No. AF 18(600)-392), Eng. Exp. Station, Univ. Ill., Apr. 1954.

25. Korst, H. H., Page, R. H., and Childs, M. E.: A Theory for Base Pressure in Transonic and Supersonic Flow. Tech. Note 392-2 (Contract No. AF 18(600)-392), Eng. Exp. Station, Univ. Ill., Mar. 1955.

26. Korst, H. H., Page, R. H., and Childs, M. E.: Compressible Two-Dimensional Jet Mixing at Constant Pressure. Tech. Note 392-3 (Contract No. AF 18(600)-392), Eng. Exp. Station, Univ. Ill., Apr. 1955.

27. Korst, H. H., and Chow, W. L.: Compressible Non-Isoenergetic Two-Dimensional Turbulent ($Pr_t = 1$) Jet Mixing at Constant Pressure - Auxiliary Integrals, Heat Transfer, and Friction Coefficients for Fully Developed Mixing Profiles. Tech. Note 392-4 (Contract No. AF 18(600)-392), Eng. Exp. Station, Univ. Ill., Aug. 1963 (second ed.).

TABLE I.- PHYSICAL CHARACTERISTICS OF THE X-15 AIRPLANE

Wing:
  Airfoil section . . . . NACA 66005 (modified)
  Total area (includes 94.98 sq ft covered by fuselage), sq ft 200
  Span, ft 22.36
  Mean aerodynamic chord, ft 10.27
  Root chord, ft 14.91
  Tip chord, ft 2.98
  Taper ratio 0.20
  Aspect ratio 2.50
  Sweep at 25-percent-chord line, deg 25.64
  Incidence, deg 0
  Dihedral, deg 0
  Aerodynamic twist, deg 0
  Flap -
    Type . . . . Plain
    Area (each), sq ft 8.30
    Span (each), ft 4.50
    Inboard chord, ft 2.61
    Outboard chord, ft 1.08

		Original	Present
Deflection, down (nominal design), deg		40	32
Ratio flap chord to wing chord			0.22
Ratio total flap area to wing area			0.08
Ratio flap span to wing semispan			0.40
Trailing-edge angle, deg			5.67
Sweepback angle of hinge line, deg			0

Horizontal tail:
  Airfoil section . . . . NACA 66005 (modified)
  Total area (includes 63.29 sq ft covered by fuselage), sq ft 115.34
  Span, ft 18.08
  Mean aerodynamic chord, ft 7.05
  Root chord, ft 10.22
  Tip chord, ft 2.11
  Taper ratio 0.21
  Aspect ratio 2.83
  Sweep at 25-percent-chord line, deg 45
  Dihedral, deg . . . . -15
  Ratio horizontal-tail area to wing area 0.58
  Movable surface area, sq ft 51.77
  Deflection -
    Longitudinal, up, deg 15
    Longitudinal, down, deg 35
    Lateral differential (pilot authority), deg . . . . ±15
    Lateral differential (autopilot authority), deg . . . . ±30
  Control system . . . . Irreversible hydraulic boost with artificial feel

Upper vertical tail:
  Airfoil section . . . . 10° single wedge
  Total area, sq ft 40.91
  Span, ft 4.58
  Mean aerodynamic chord, ft 8.95
  Root chord, ft 10.21
  Tip chord, ft 7.56
  Taper ratio 0.74
  Aspect ratio 0.51
  Sweep at 25-percent-chord line, deg 23.41

TABLE I.- PHYSICAL CHARACTERISTICS OF THE X-15 AIRPLANE - Concluded

Ratio vertical-tail area to wing area 0.20
Movable surface area, sq ft 26.45
Deflection, deg . . . . ±7.50
Sweepback of hinge line, deg   0
Control system . . . .   Irreversible hydraulic boost with artificial feel

Lower vertical tail:
  Airfoil section . . . . 10° single wedge
  Total area, sq ft 34.41
  Span, ft 3.83
  Mean aerodynamic chord, ft 9.17
  Root chord, ft 10.21
  Tip chord, ft   8
  Taper ratio 0.78
  Aspect ratio 0.43
  Sweep at 25-percent-chord line, deg 23.41
  Ratio vertical-tail area to wing area 0.17
  Movable surface area, sq ft 19.95
  Deflection, deg . . . . ±7.50
  Sweepback of hinge line, deg   0
  Control system . . . .   Irreversible hydraulic boost with artificial feel

Fuselage:
  Length, ft 49.17
  Maximum width, ft 7.33
  Maximum depth, ft 4.67
  Maximum depth over canopy, ft 4.97
  Side area (total), sq ft 215.66
  Fineness ratio 10.91

TABLE II.- PHYSICAL CHARACTERISTICS OF ROCKET ENGINE AND BASE ELEMENTS

Boattail angle, deg 6.3

Base areas, sq ft:
  Upper vertical fin 4.7
  Lower (jettisonable) vertical fin 3.4
  Stationary fins, speed-brake regions (both) 6.7
  Side fairings (both) 4.8
  Fuselage (power off) 12.6
  Fuselage (power on) 8.5
  Wing (both) 1.1
  Horizontal tail (both) 0.5
  Landing gear, retracted (both) 0.3

Linear dimensions pertinent to orifices:

Orifice	c, in.	h, in.	l, in.
1	93	17.0	19.5
2	102	18.6	19.5
3	109	19.9	19.5
4	116	21.1	19.5
5	591	Not applicable	-0.5
6	575	Not applicable	28.0
7	109	1.06	160.0
8	116	21.1	19.5

Engine, single chamber:
  Throat area, sq in. 58.6
  Jet-exit area, sq in. 578
  Turbine exhaust area, sq in. 20
  Nozzle half-angle, deg 20
  Chamber pressure, for full throttle, design, psia 600
  Fuel . . . . Ammonia
  Oxidizer . . . . Liquid oxygen
  Fuel-oxidizer ratio, by weight 1.25
  Ratio of specific heat 1.23
  Thrust, lb . . . . Throttleable from 28,500 to 58,500
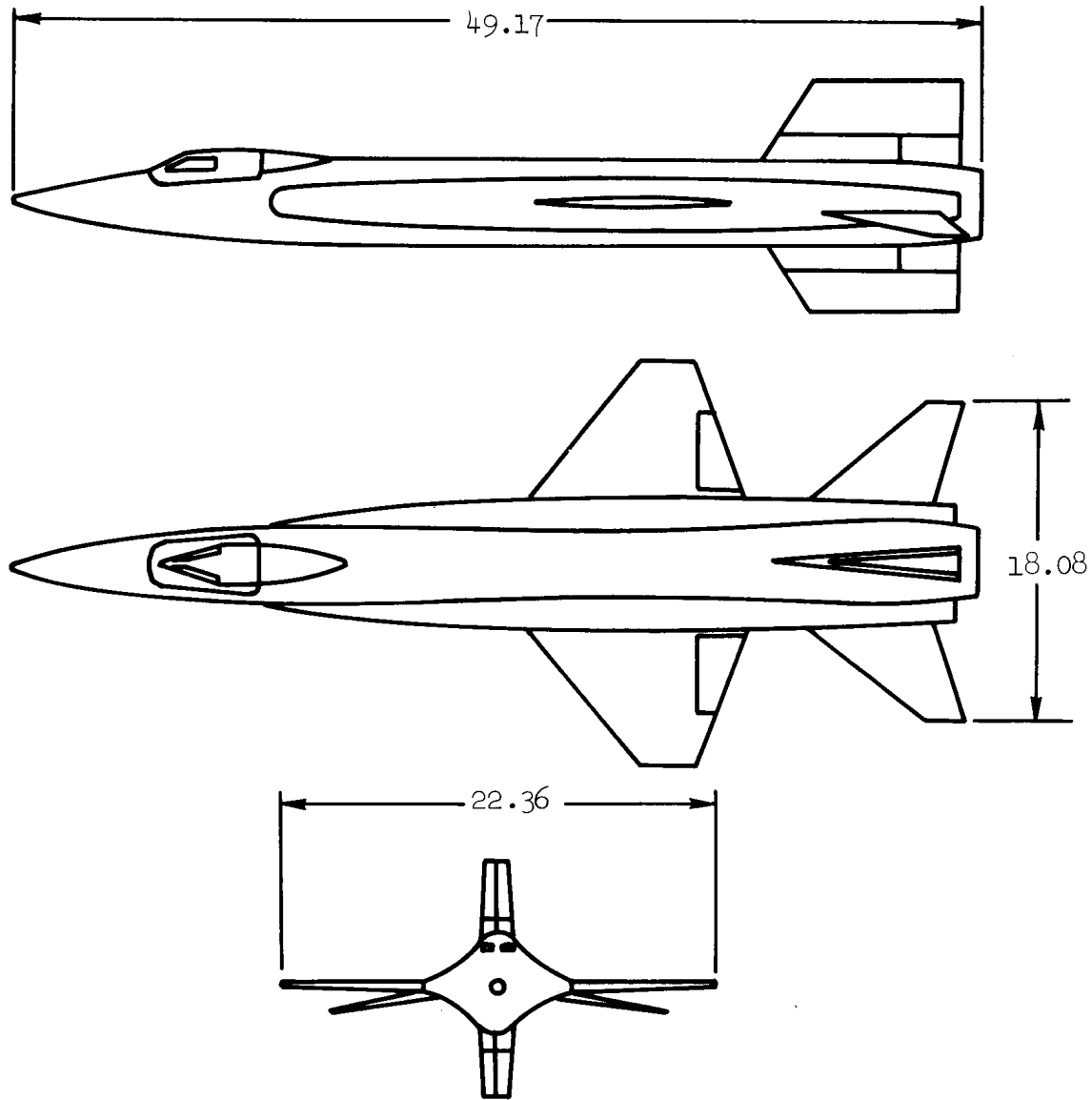
Figure 1.- Three-view drawing of the X-15 airplane.
Dimensions in feet.
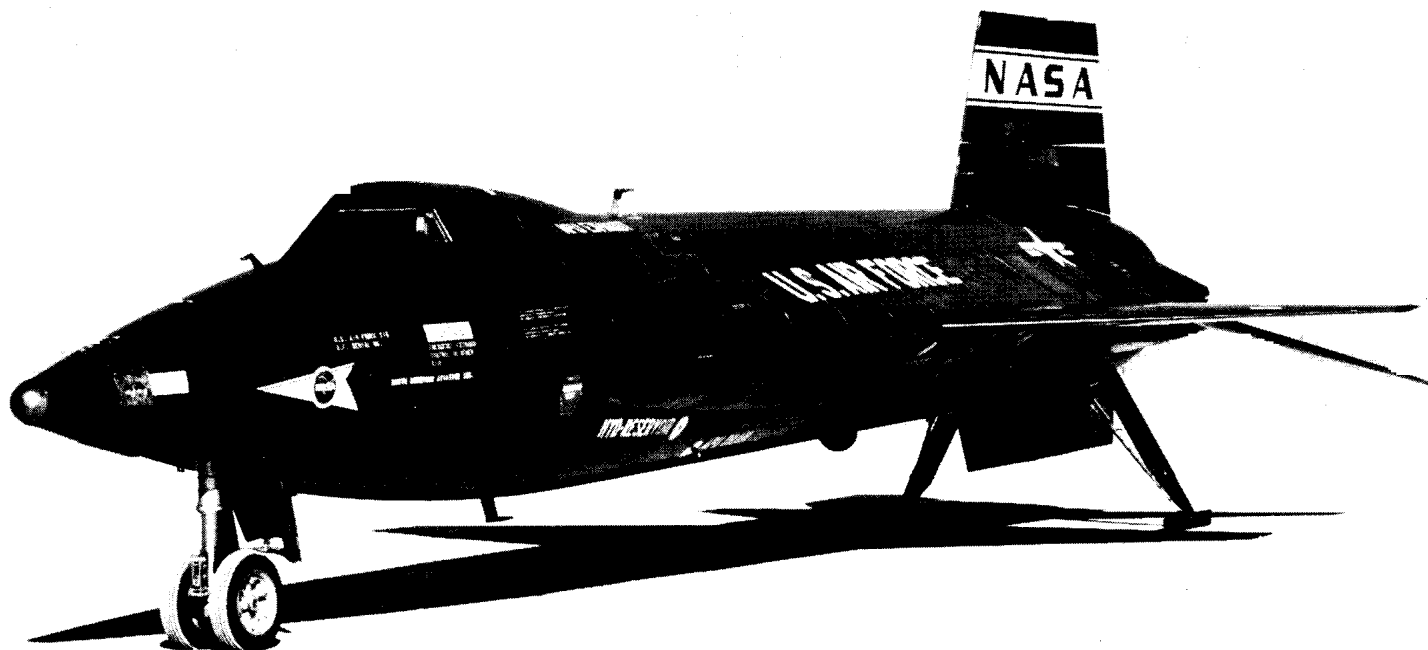
Figure 2.- X-15 airplane.

E-7902

Flameshield

Outline of speed brakes
when full open
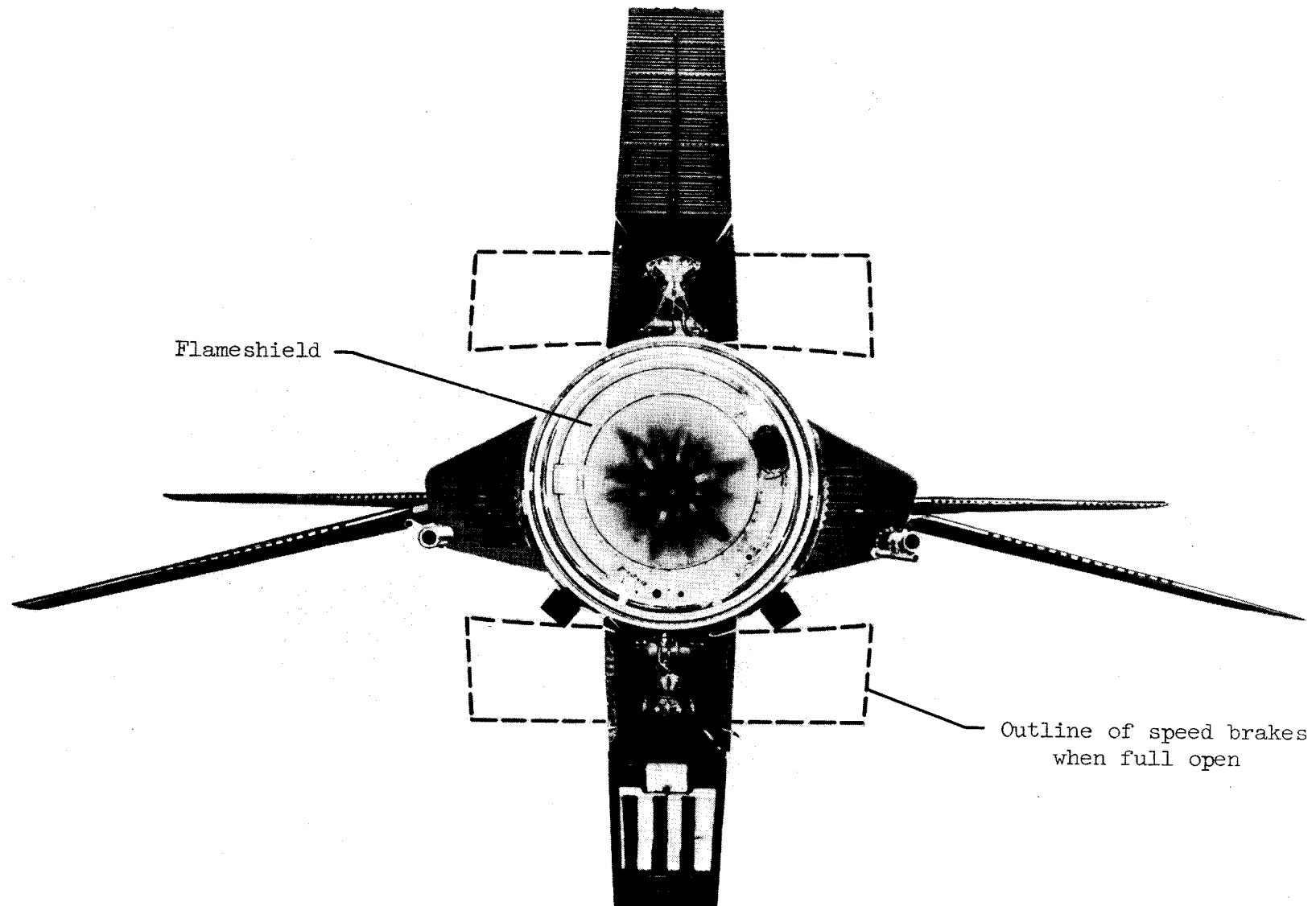
E-7101

Figure 3.- Base region of the X-15 airplane as it existed for the present study.
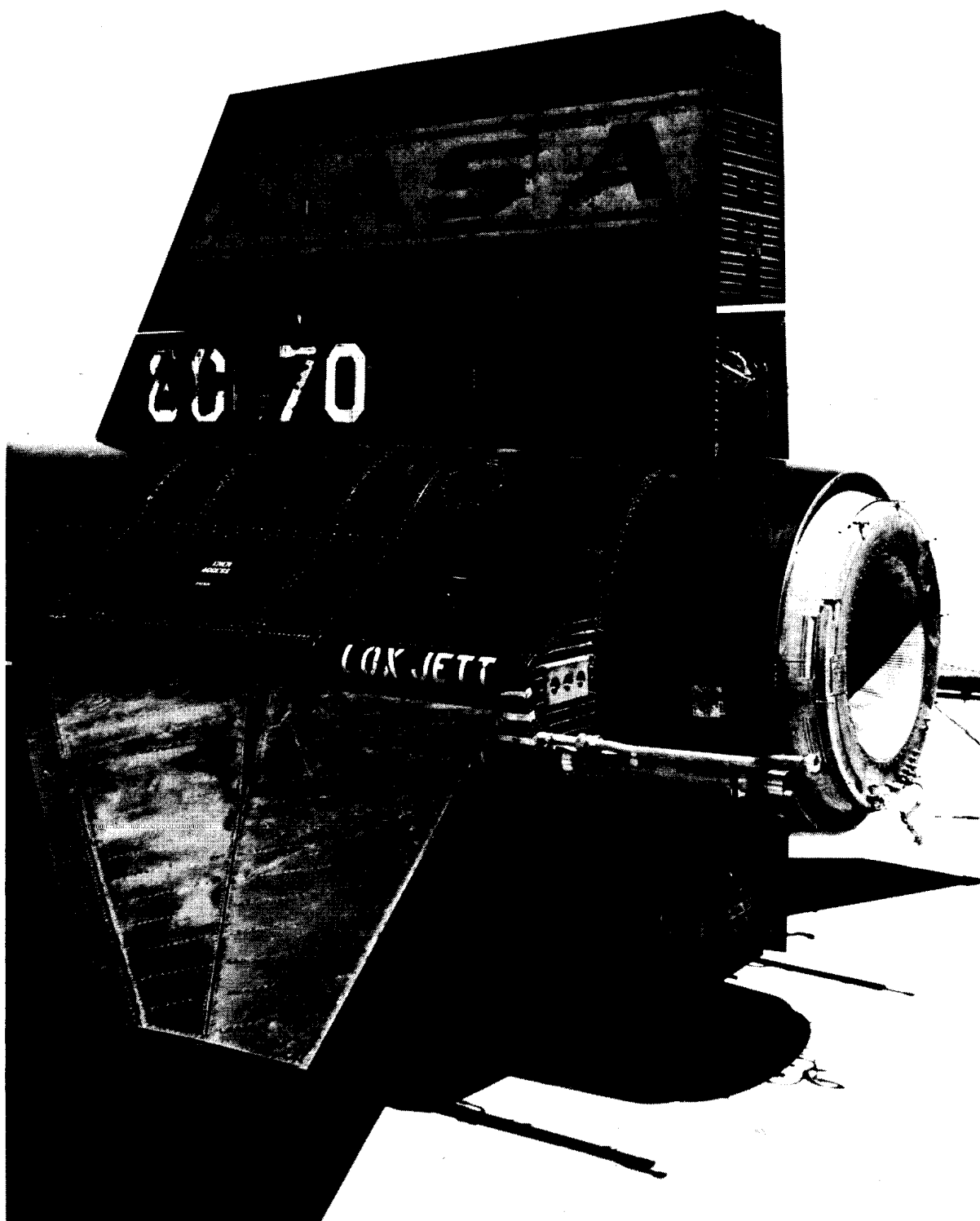
Figure 4.- X-15 viewed from the left rear. Lower jettisonable fin removed.
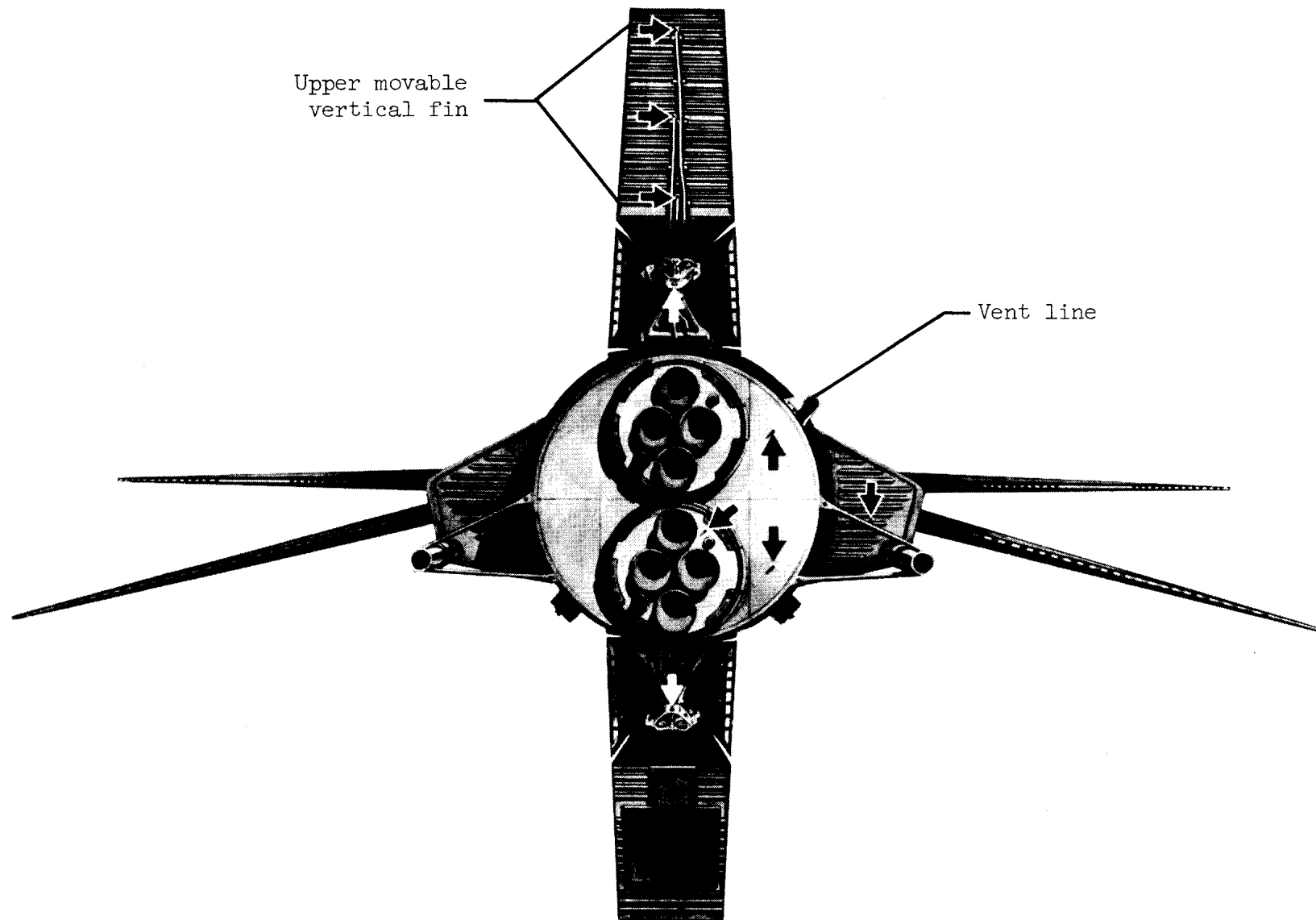
Figure 5.- Rear view of X-15 with interim rocket engine installation.
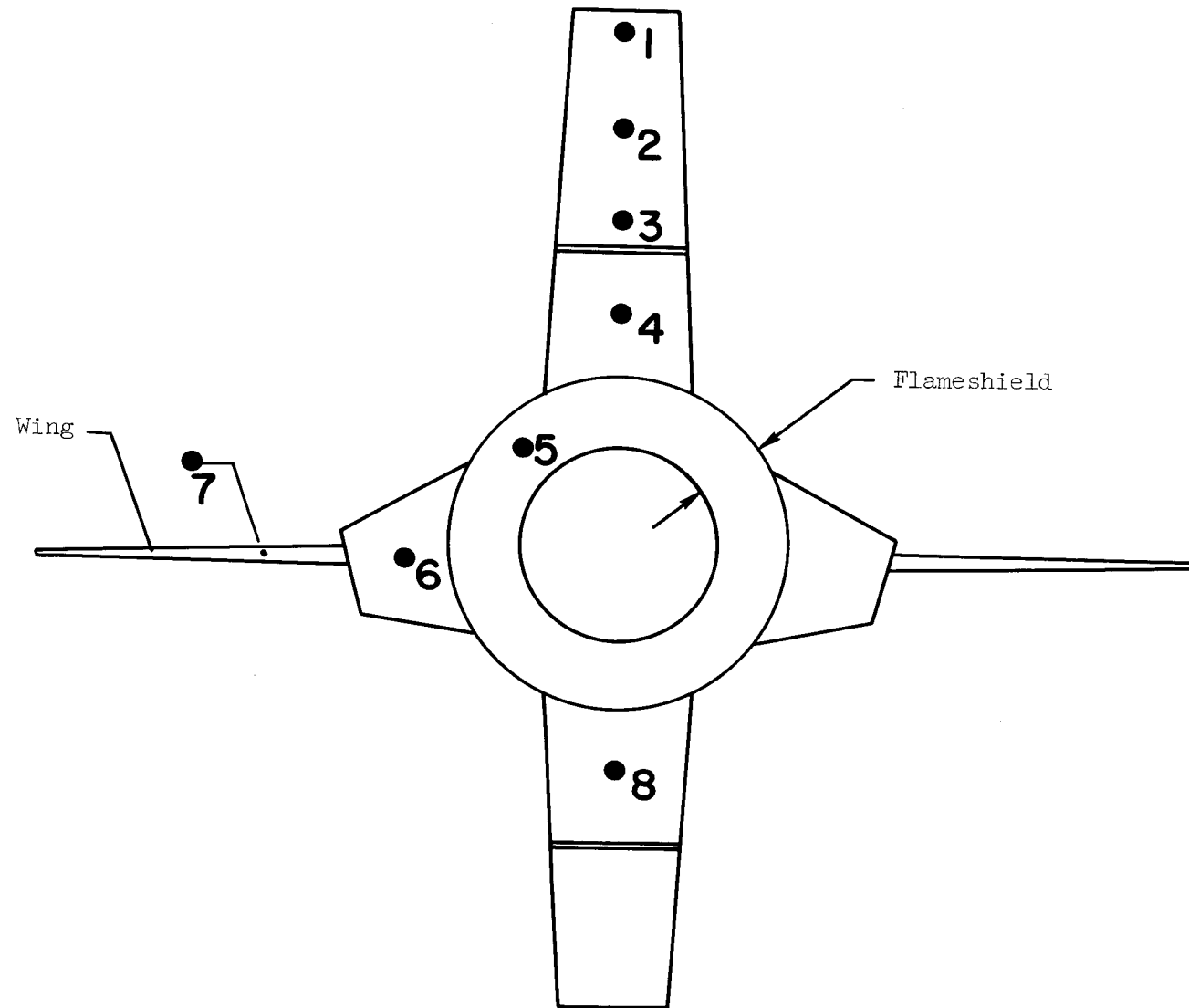
Figure 6.- Schematic drawing of X-15 base showing location of orifices.
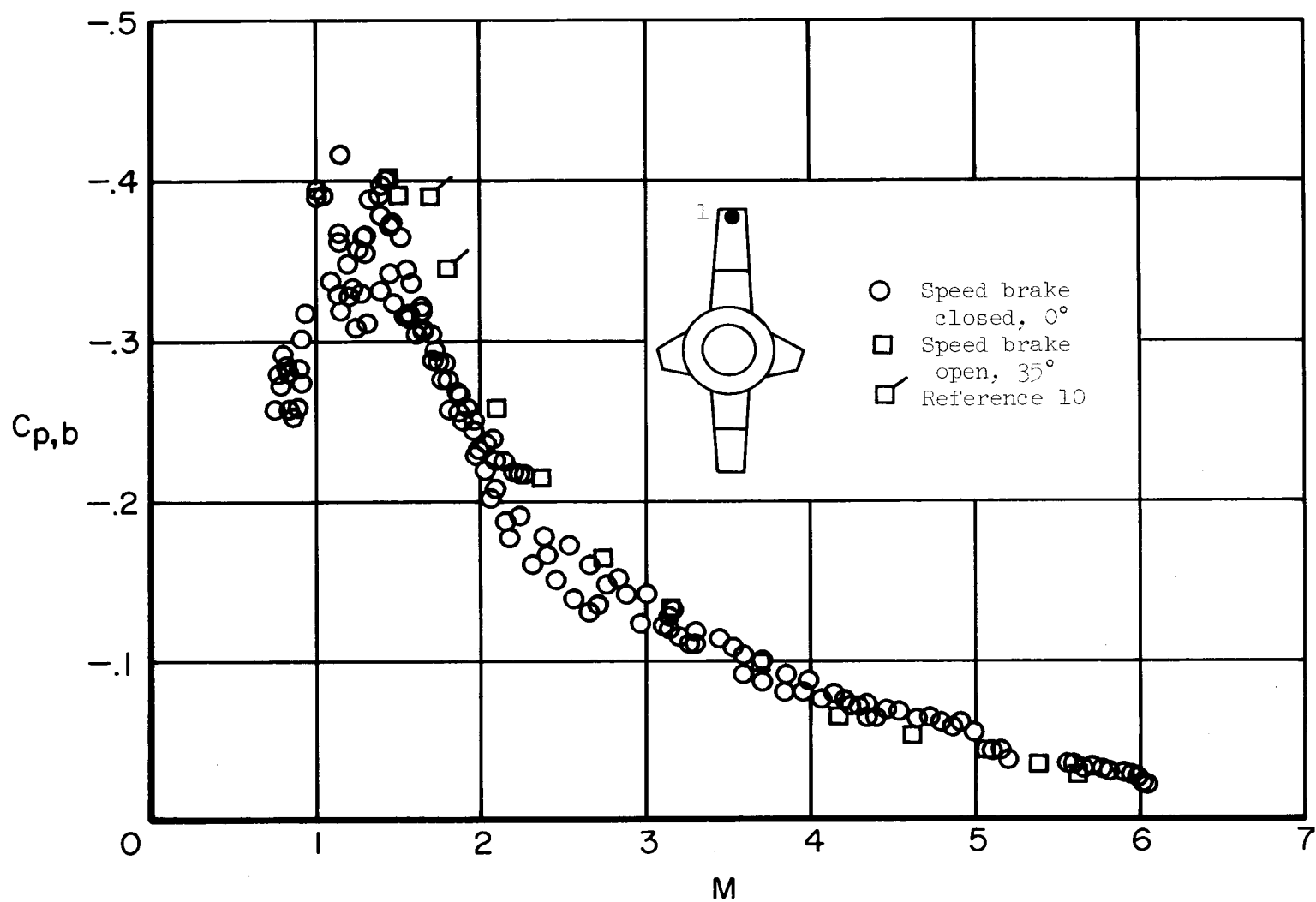
(a) Top of upper movable vertical fin.

Figure 7.- Variation of base pressure coefficient with free-stream Mach number.
Power off except where indicated otherwise.
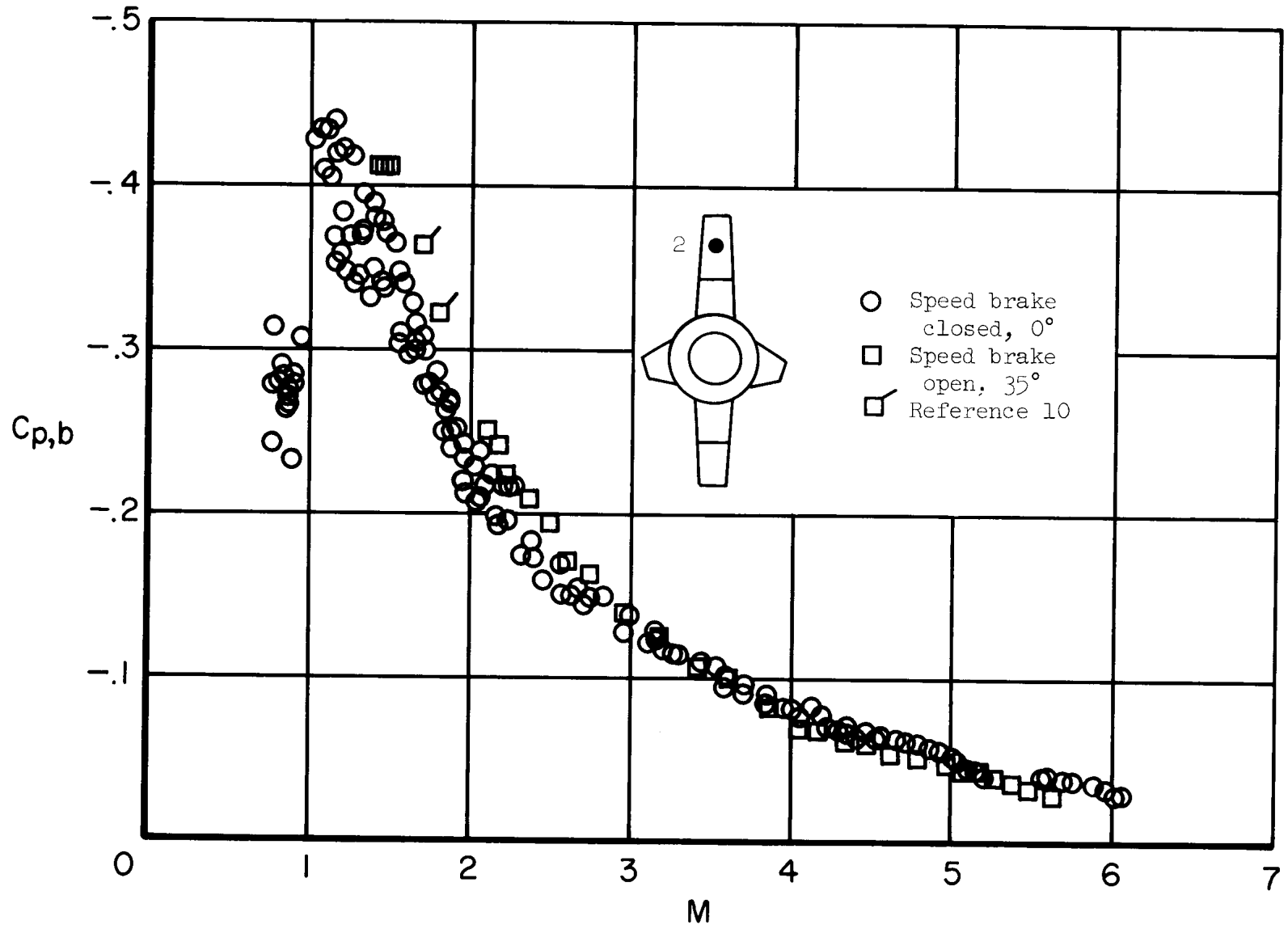
(b) Center of upper movable vertical fin.
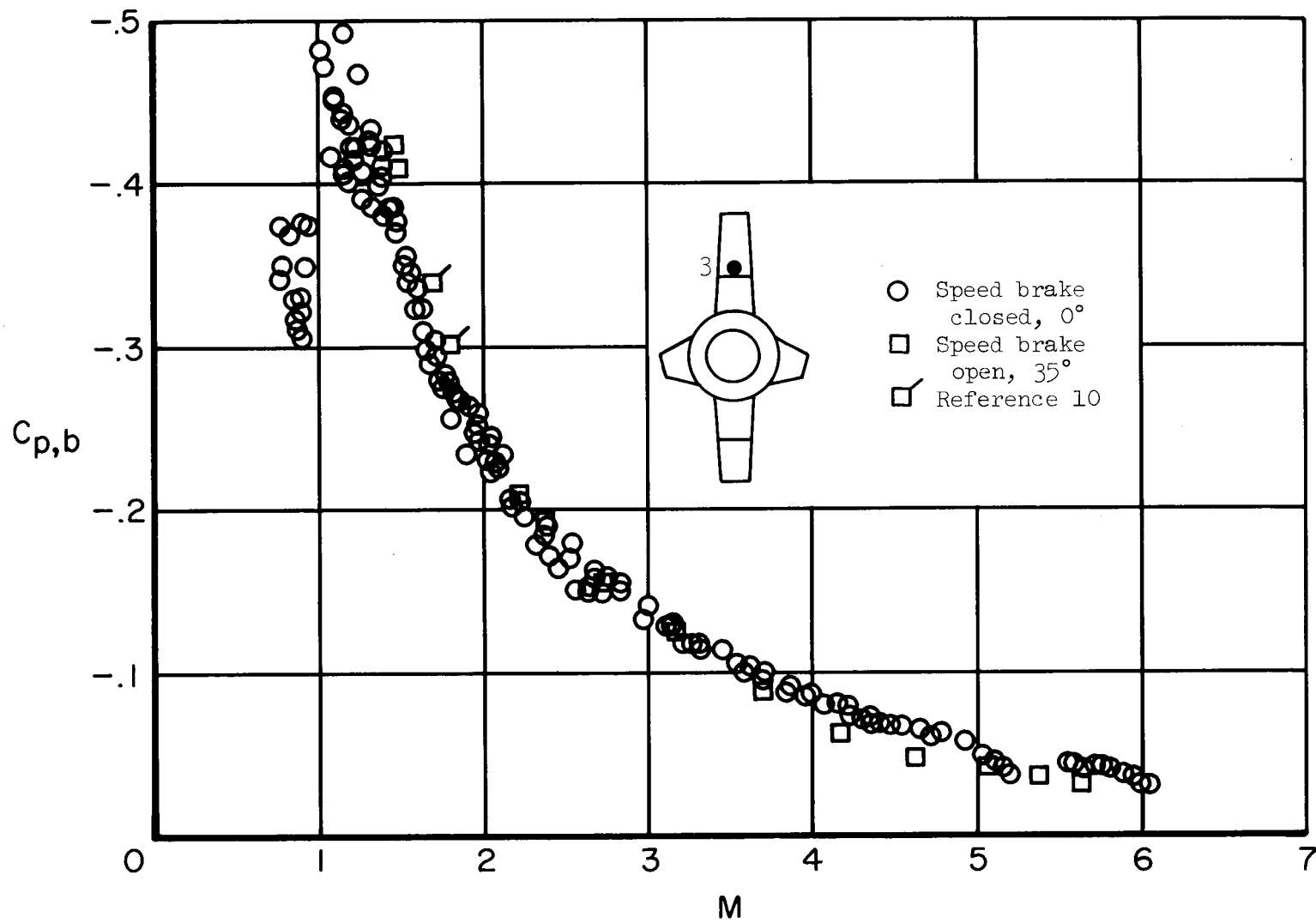
Figure 7.- Continued.

(c) Bottom of upper movable vertical fin.
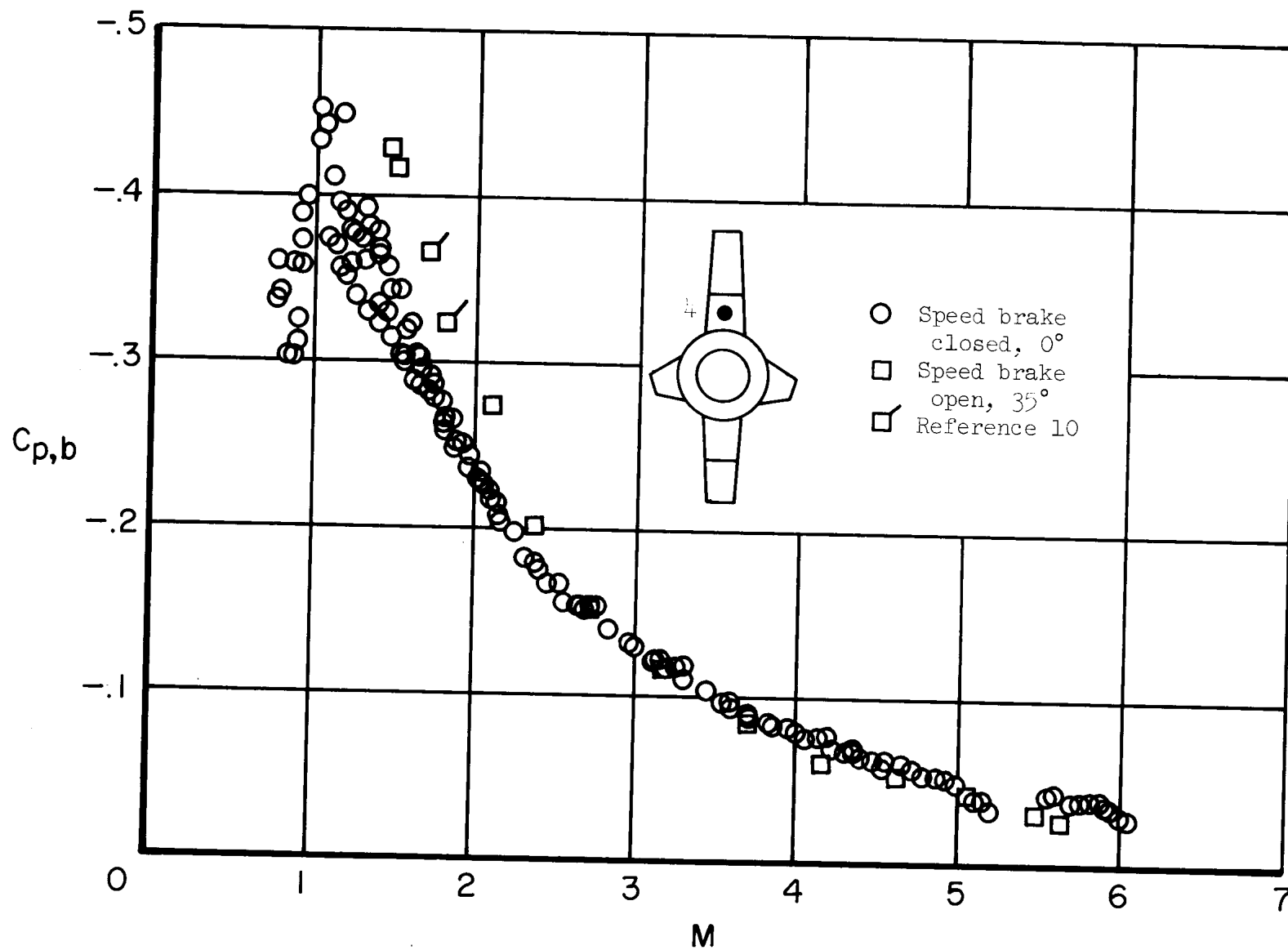
Figure 7.- Continued.

(d) Upper fixed vertical fin.
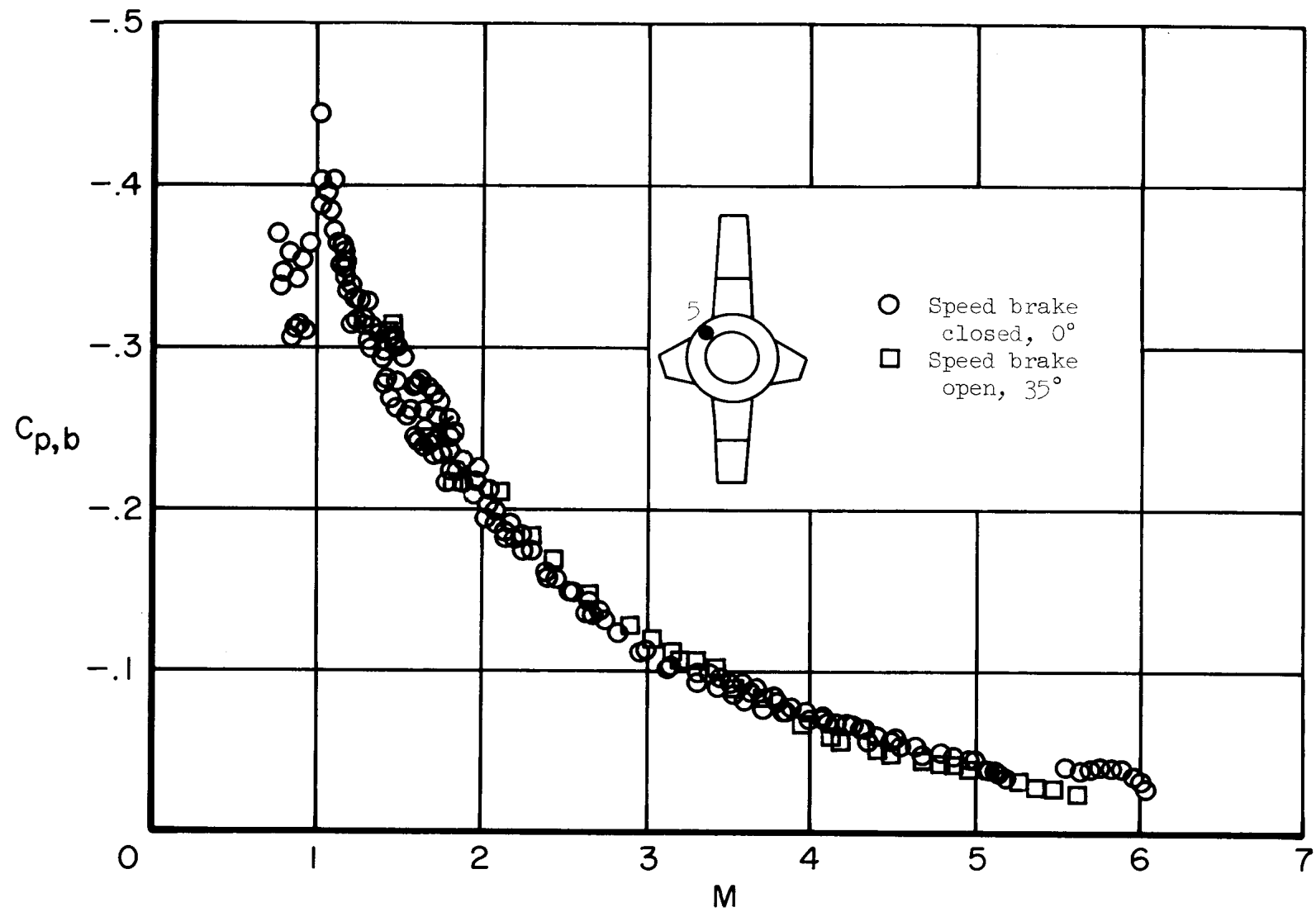
Figure 7.- Continued.

(e) Fuselage flameshield

Figure 7.- Continued.
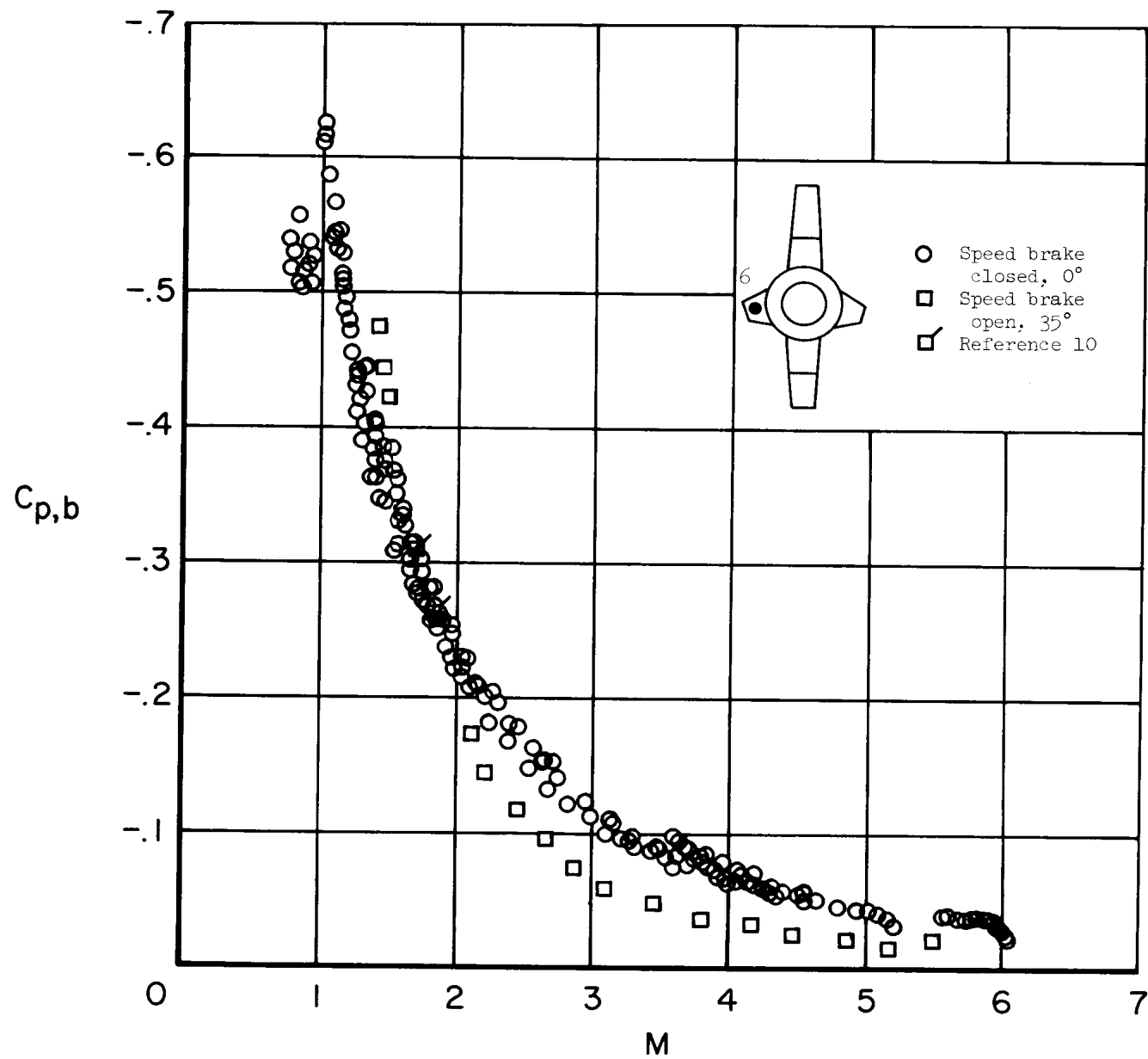
(f) Side fairing.

Figure 7.- Continued.
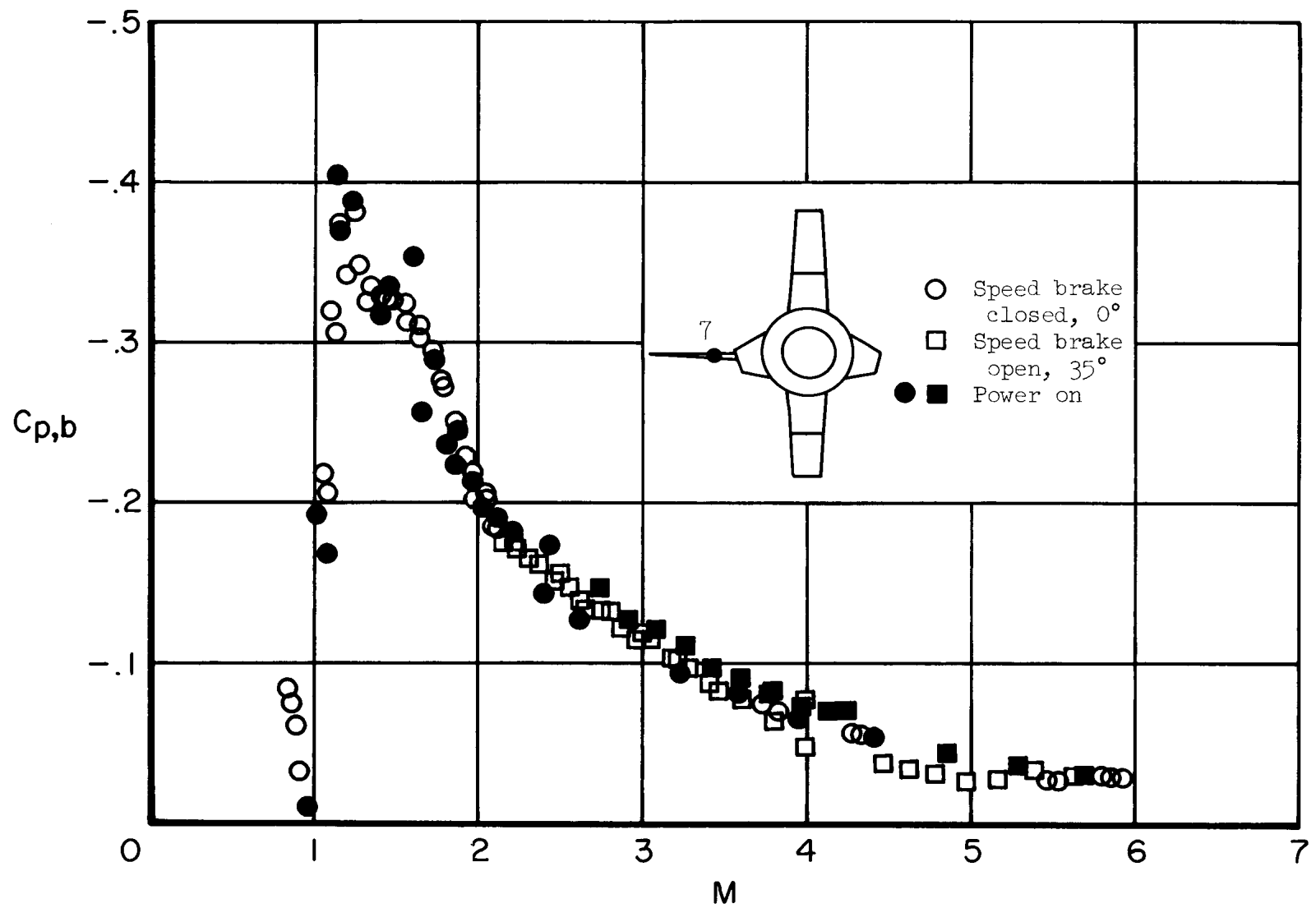
(g) Wing trailing edge (base).

Figure 7.- Continued.
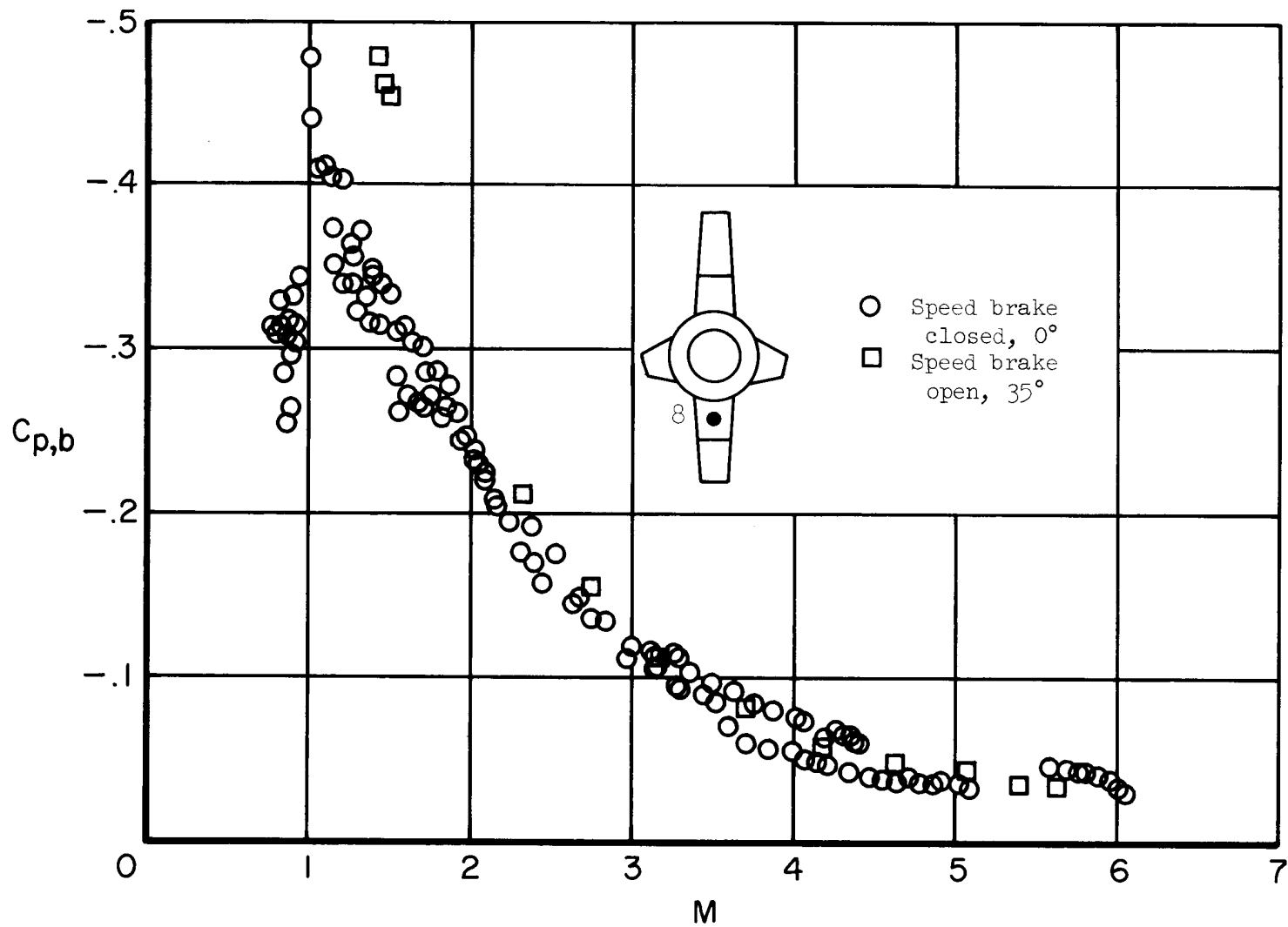
(h) Lower fixed vertical fin.

Figure 7.- Concluded.
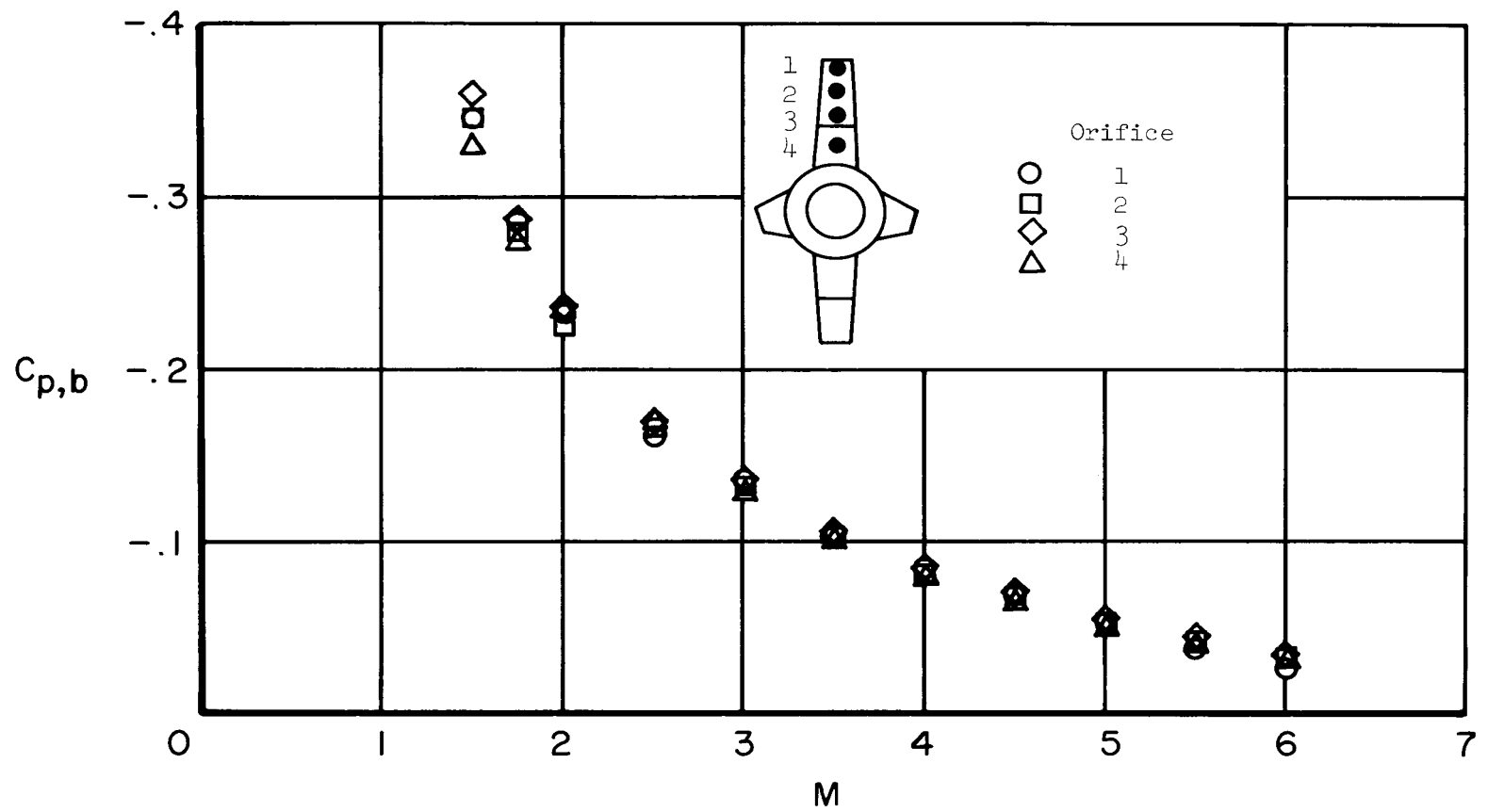
Figure 8.- Comparison of the variation of base pressure coefficient with Mach number. Power off.
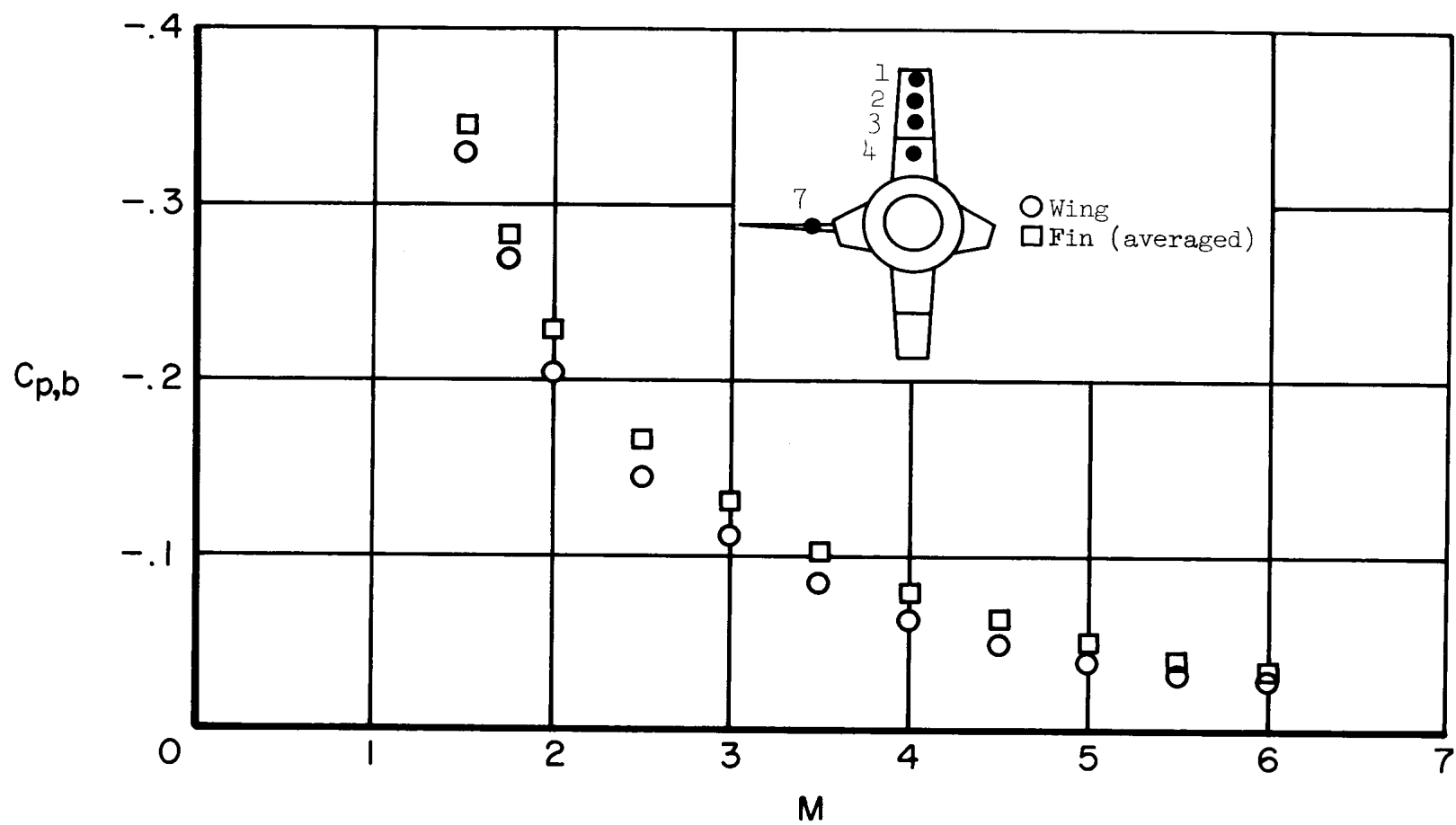
Figure 9.- Comparison of the variation of base pressure coefficient with Mach number. Power off.

	Flight		Wind tunnel
	Present tests		Reference 2
M	Fin	Wing	
1.5	$\bigcirc$	$\bullet$	————————
2.0	$\square$	$\blacksquare$	——— ——— ———
3.1	$\diamondsuit$	$\blacklozenge$	—— — —— — ——
c, in.	102	109	3
c/h	5.5	103	10 to 80
$N_{Re}/ft, \times 10^{-6}$	0.7 to 2.6		6.8 to 14.0
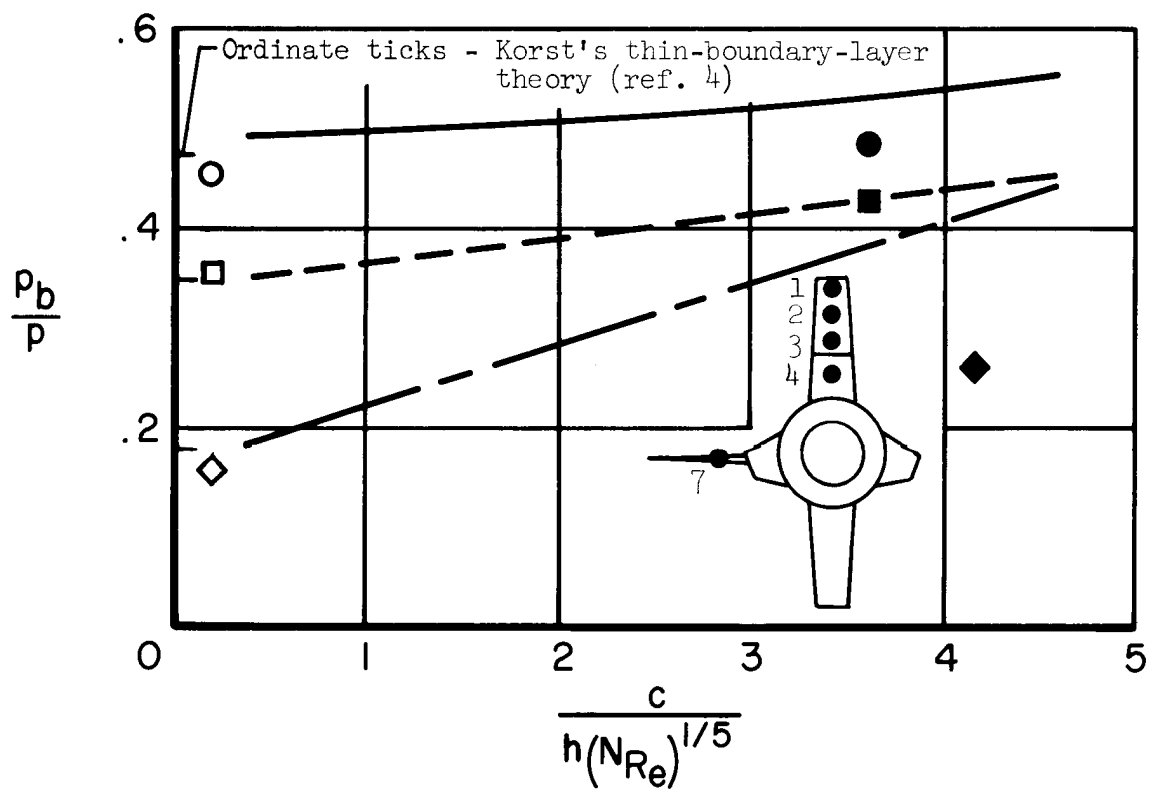
Figure 10.- Comparison of flight (power-off) vertical fin and wing base pressure ratios with wind-tunnel results for wing and theory for thin boundary layers.

		Boundary layer	$N_{Re}/ft,$ $\times 10^{-6}$	Scale
———	Flight	Turbulent[1]	0.7 to 2.6	Full
○	Ref. 15	No trip	3.8	1/15
□	Ref. 13	No trip	2.7 to 3.3	1/15
◇	Ref. 14	No trip	4.0 to 4.7	1/50
△	Ref. 11	Trip	0.9 to 2.7	1/15

[1]Caused by fabrication-type roughness and discontinuities.
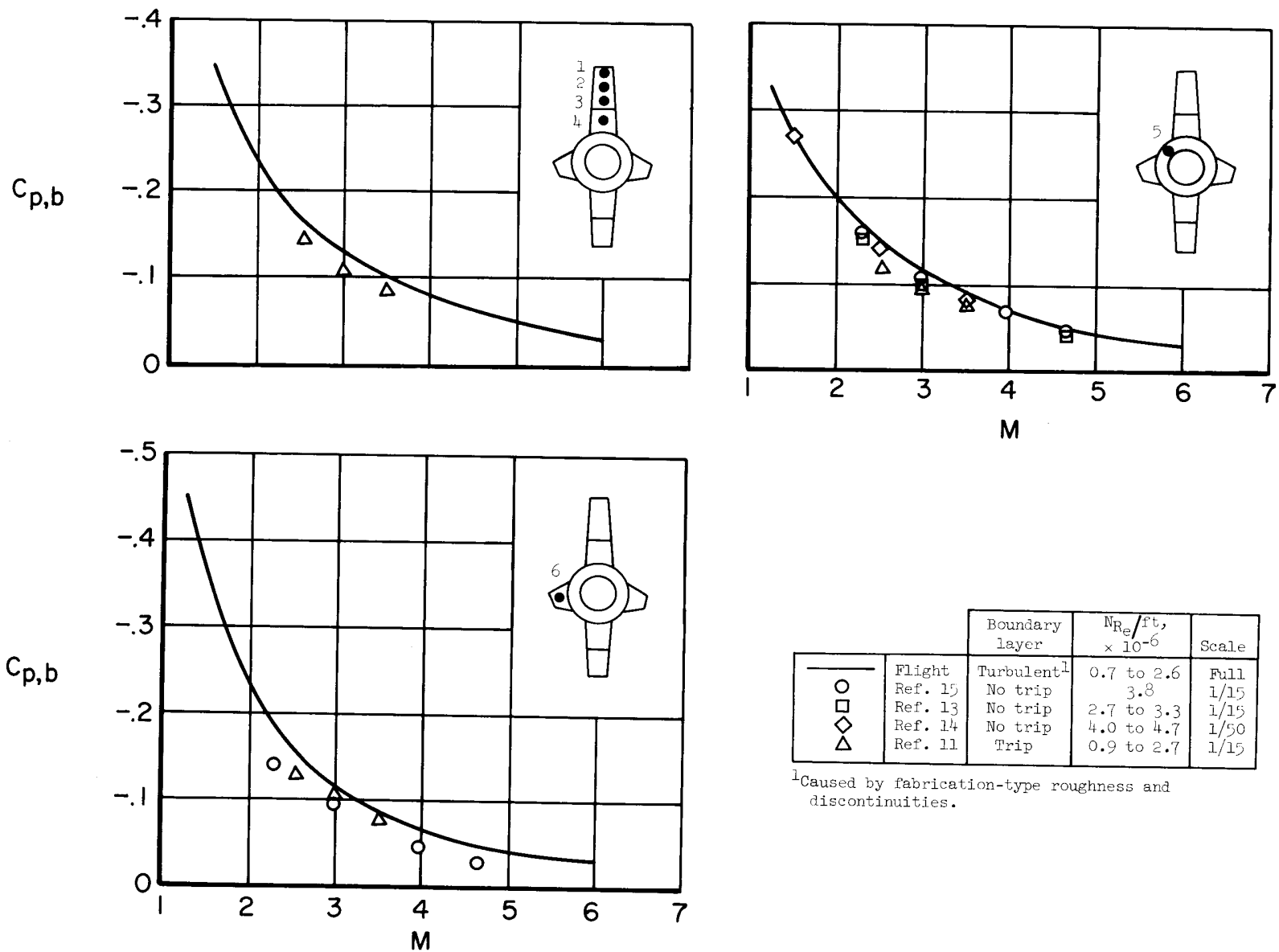
Figure 11.- Comparison of base pressure coefficients obtained from full-scale flight and X-15 wind-tunnel models. Power off.
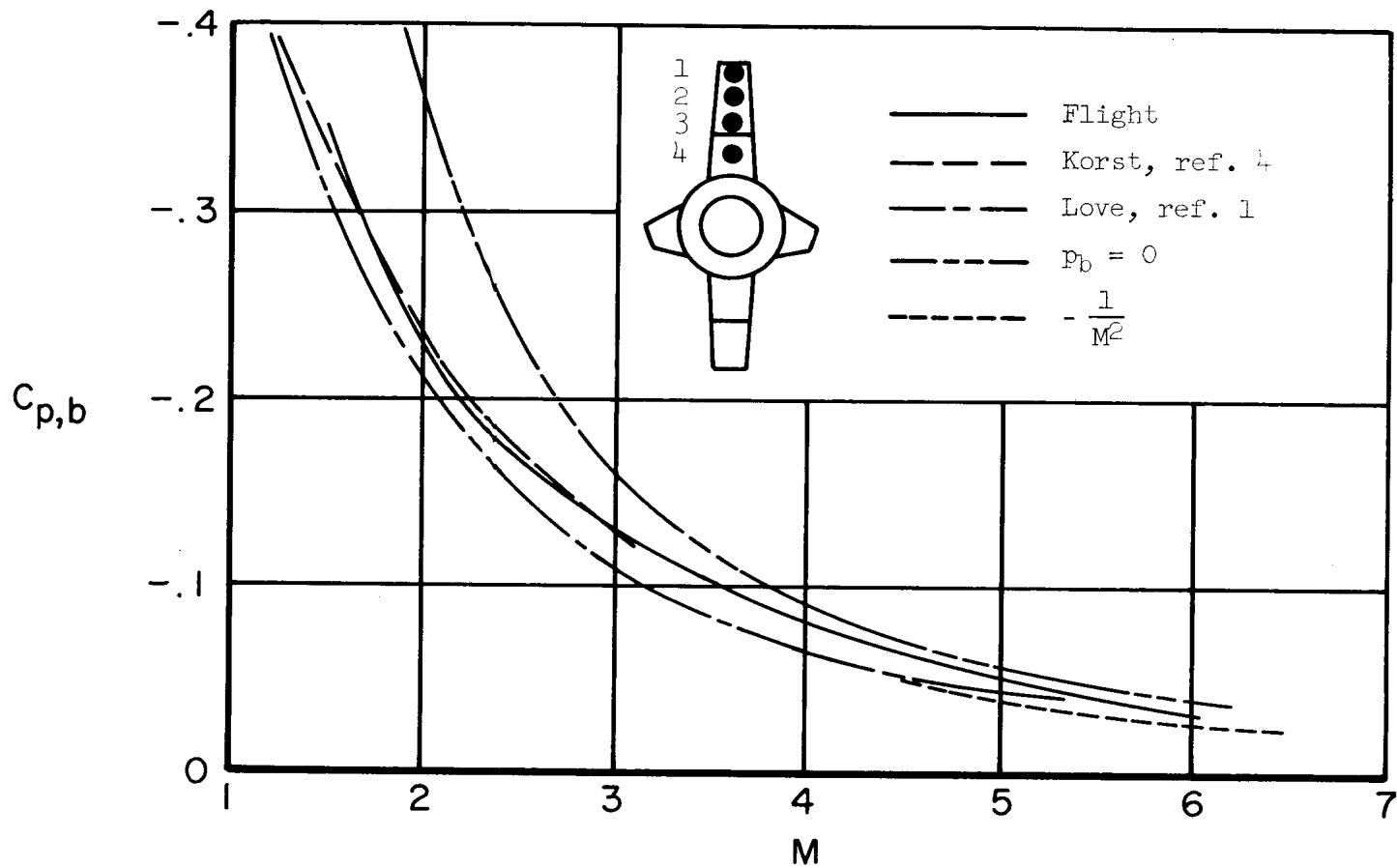
Figure 12.- Comparison of base pressure coefficient for upper vertical fin with theory for thin boundary layers and semiempirical estimate. Turbulent flow; power off for full-scale flight data.
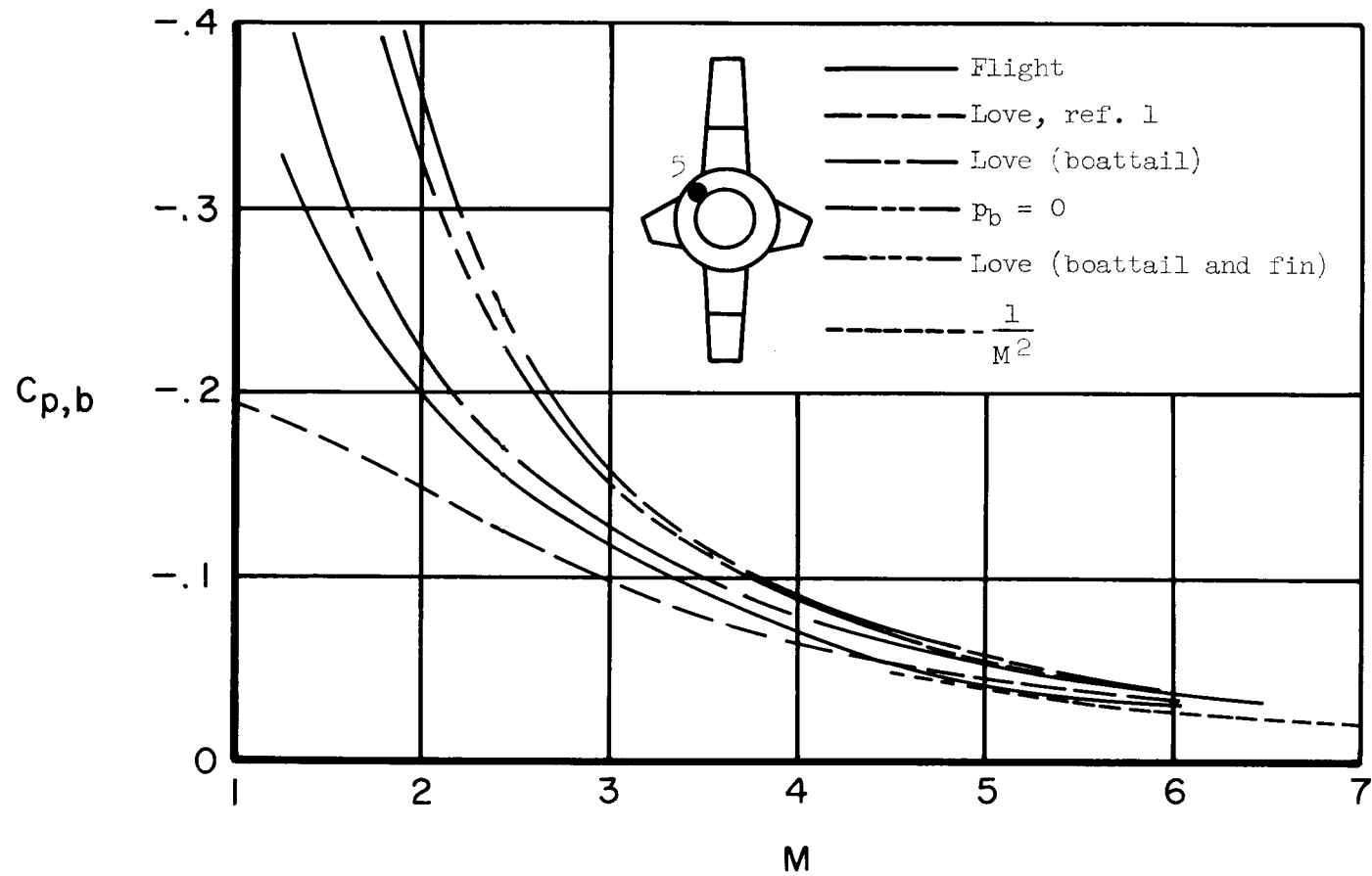
Figure 13.- Comparison of base pressure coefficient for fuselage flameshield with semiempirical estimates. Turbulent flow; power off for full-scale flight data.
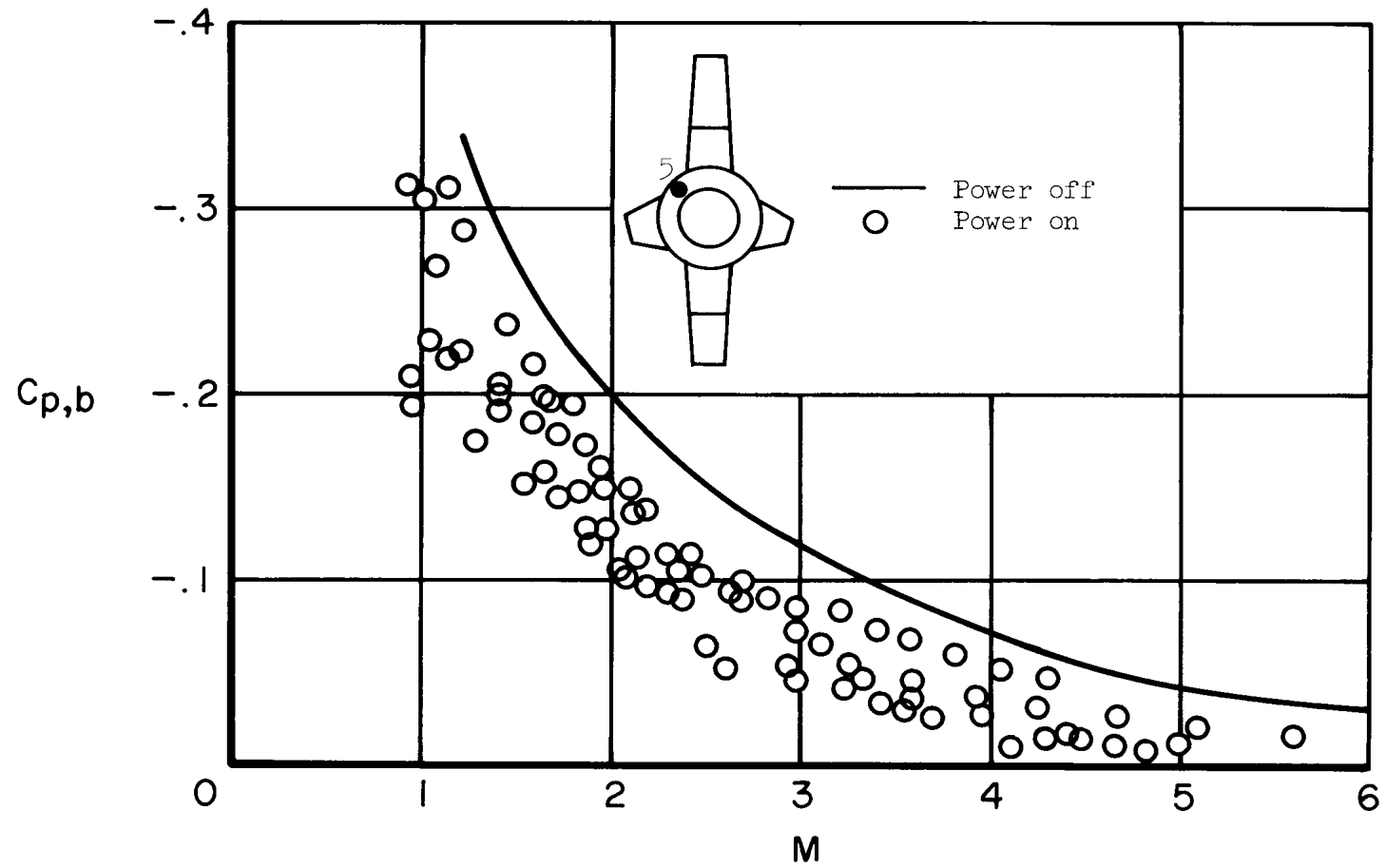
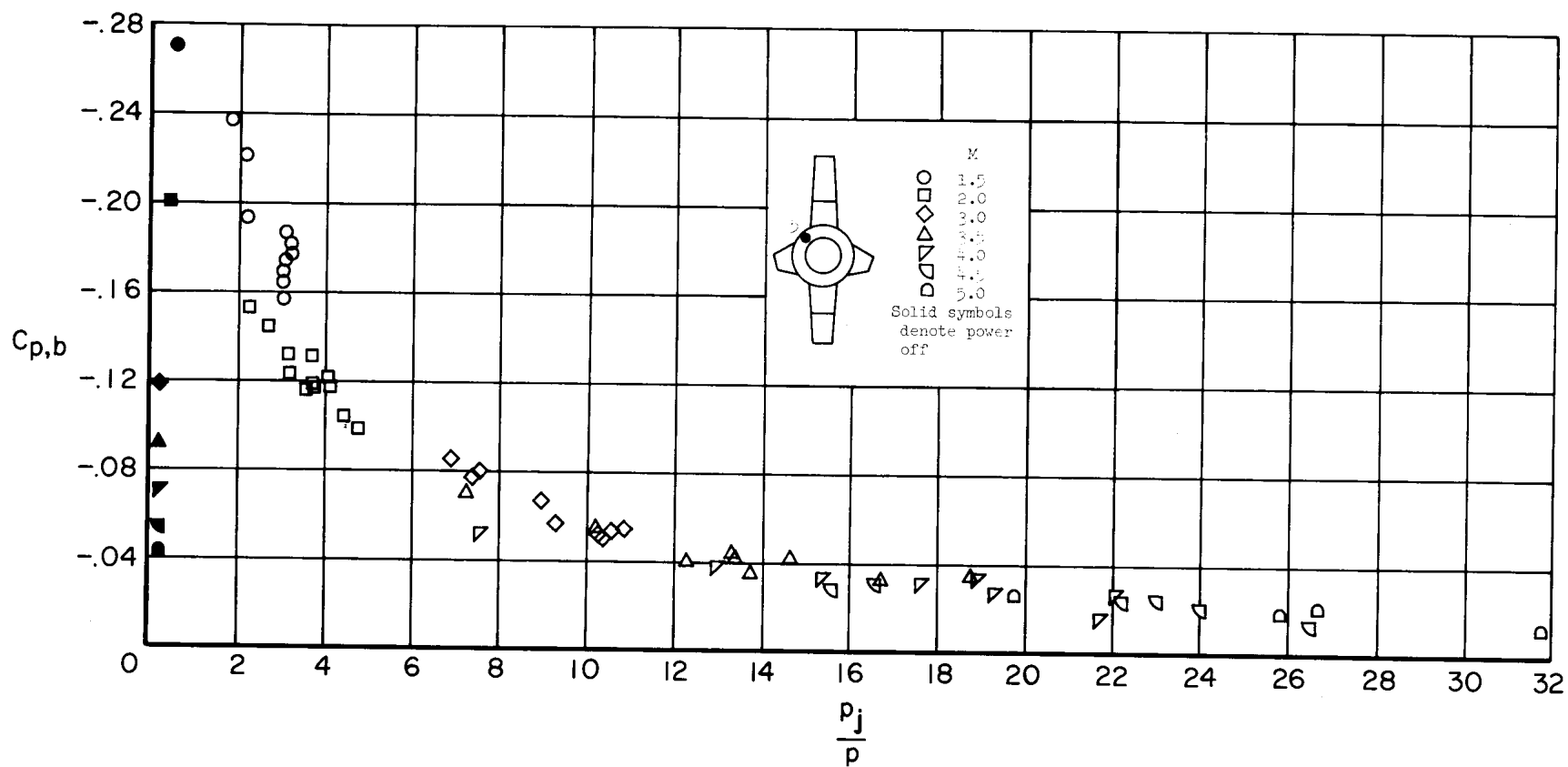Figure 14.- Relationship of power-off and power-on base pressure coefficients.

Figure 15.- Relationship of base pressure coefficient to the ratio of jet exit to free-stream static pressure.
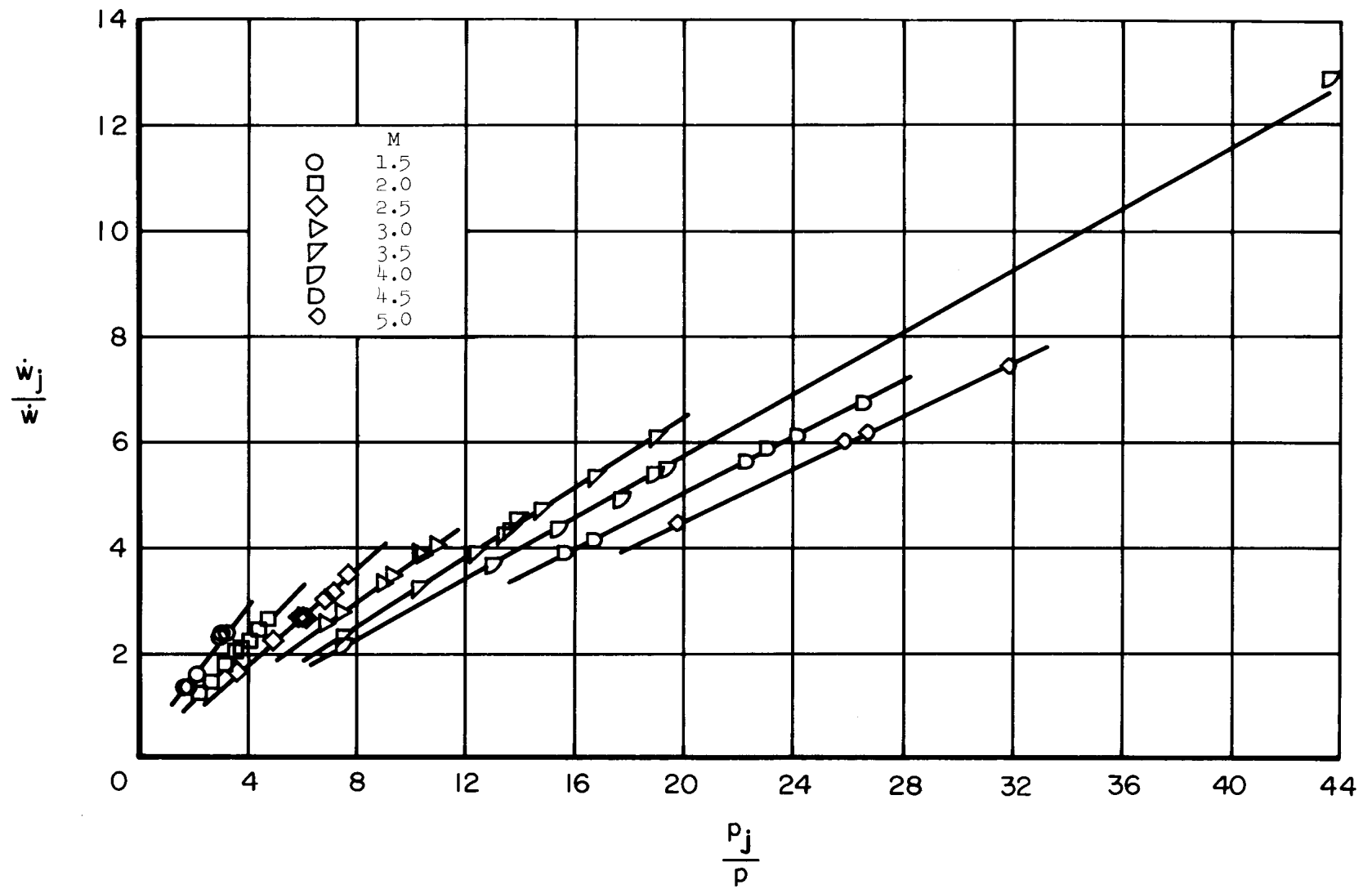
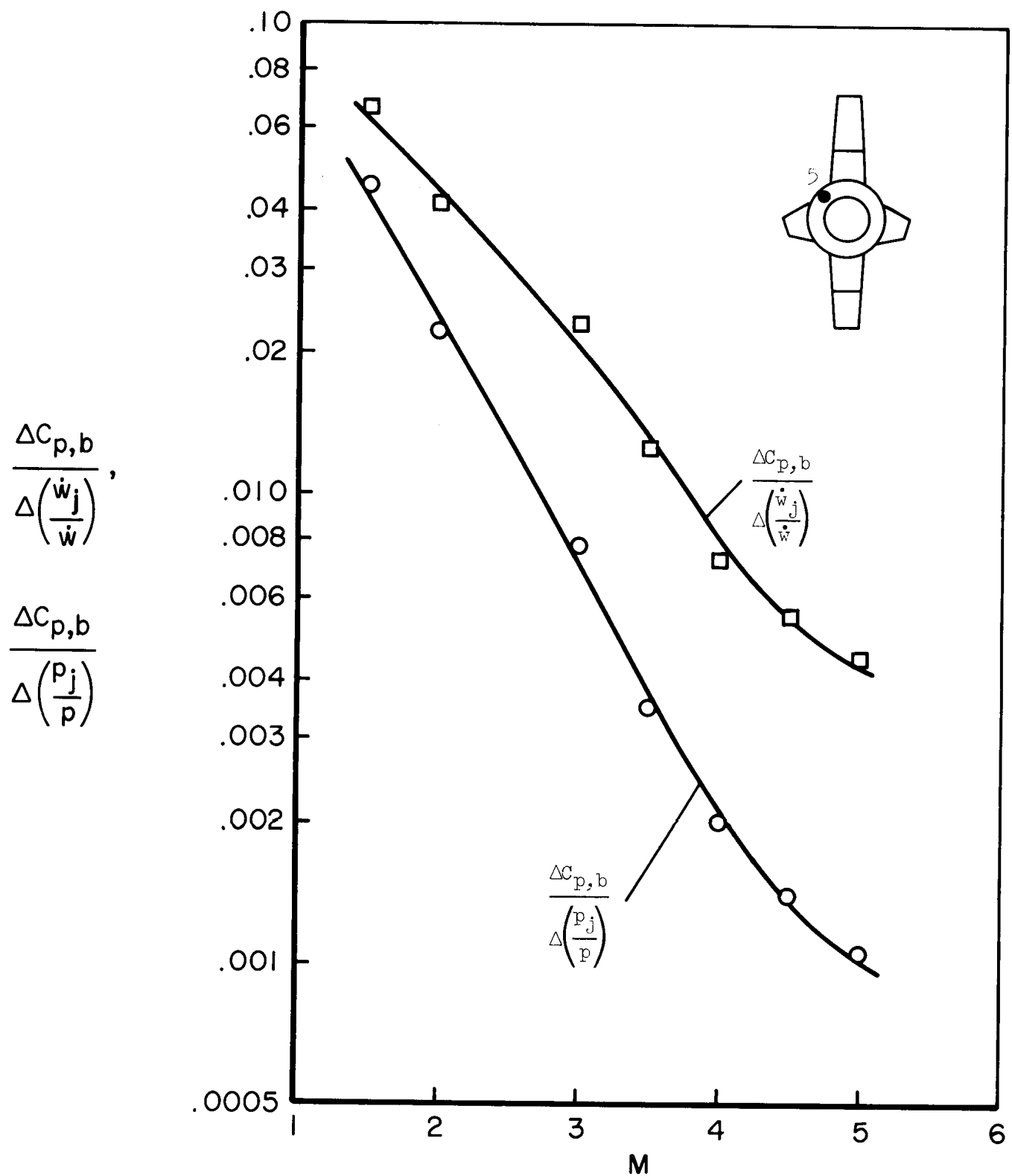Figure 16.- Relationship of mass-flow ratio to ratio of jet exit to free-stream static pressure for constant values of free-stream Mach number.

Figure 17.- Slope of base pressure coefficient with respect to jet exit flow parameters as a function of free-stream Mach number.
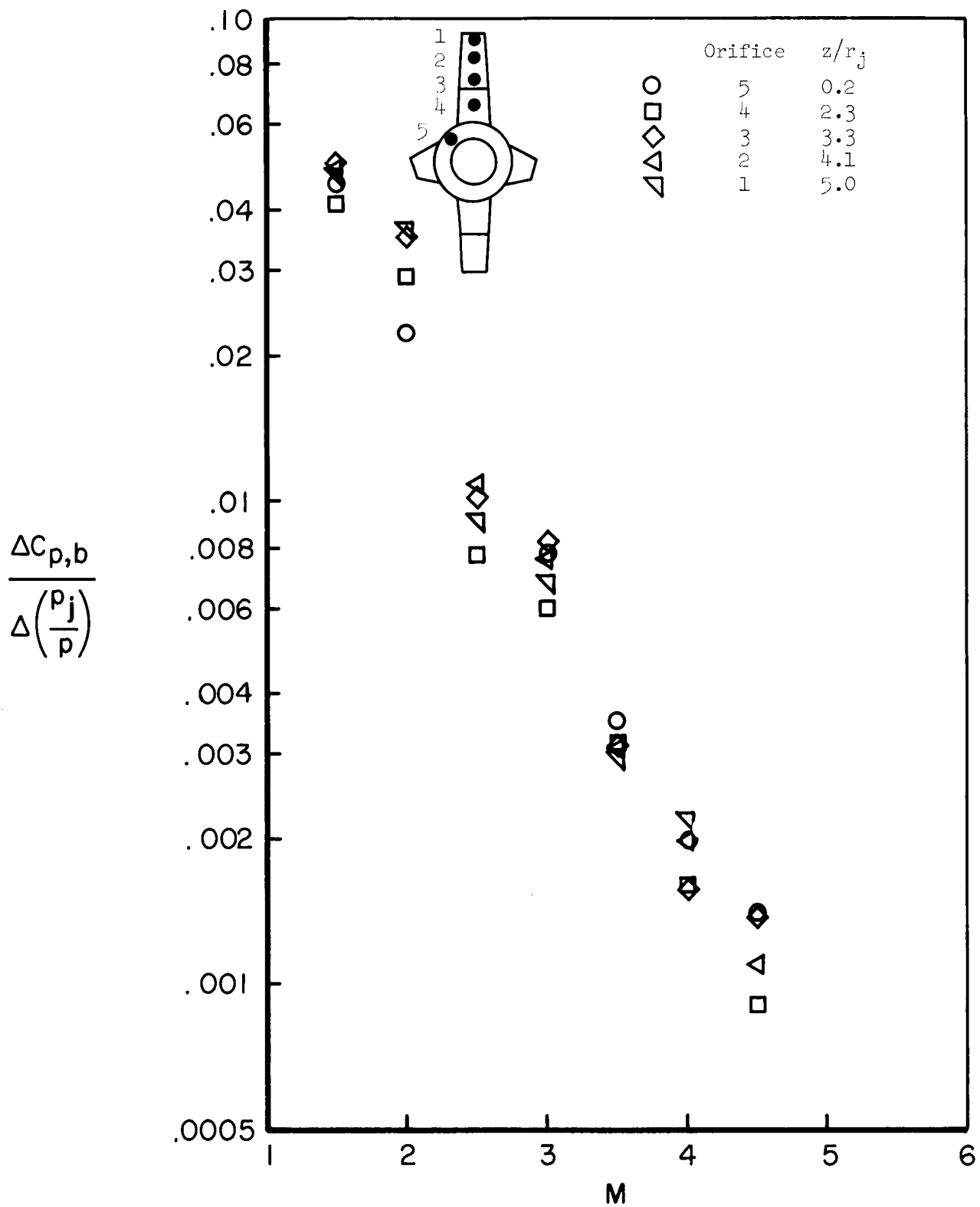
Figure 18.- Slope of base pressure coefficient with respect to ratio of jet exit to free-stream static pressure as a function of free-stream Mach number.

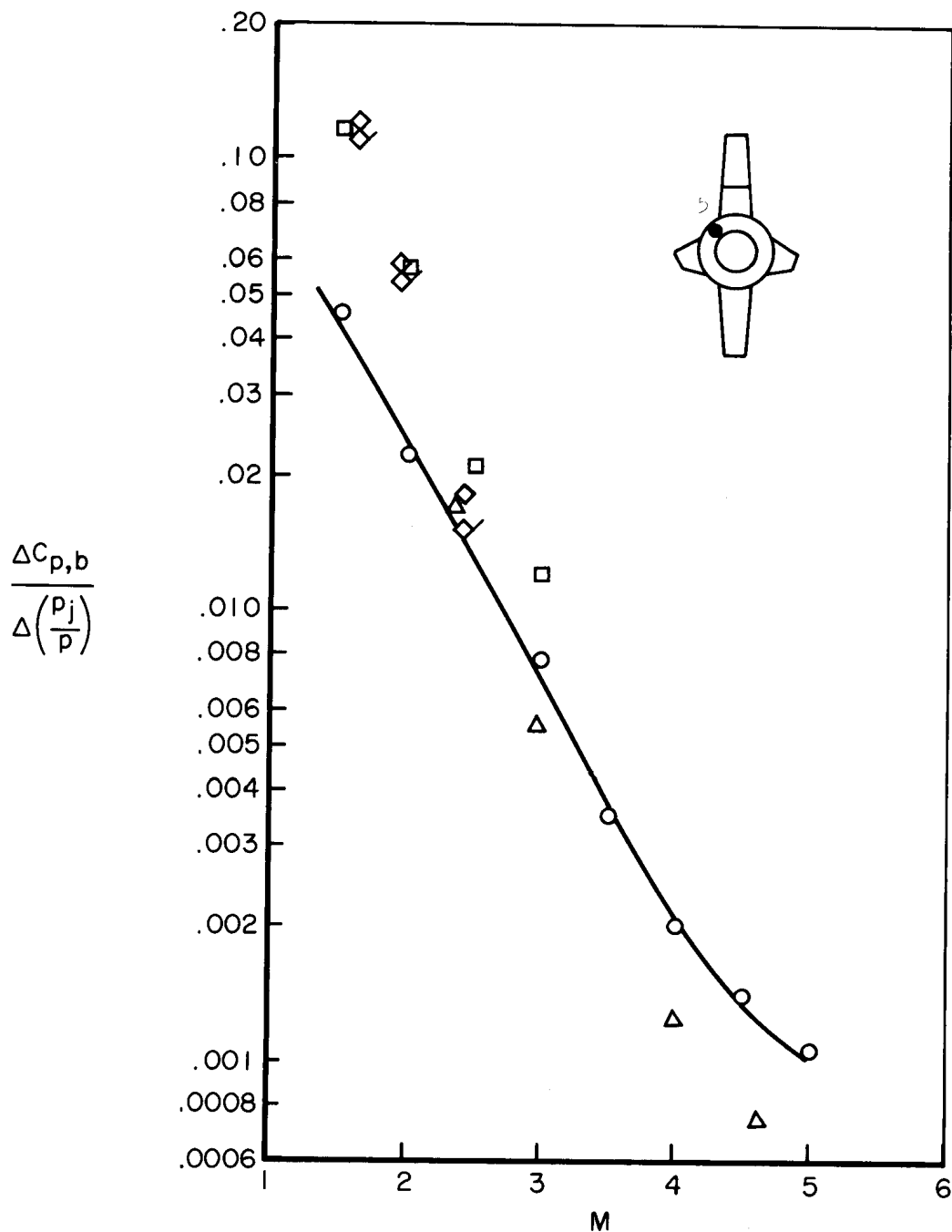|		$\dfrac{d_f}{d_j}$	β, deg	M_j	γ_j, deg
○	Flight	2.06	6.3	3.31	1.23
□	Ref. 21	2.00	6.3	----	≈1.25
◇	Ref. 19	1.33	0	3.00	1.40
◇	Ref. 19	1.33	0	3.50	1.40
△	Ref. 20	2.28	0	3.17	1.40

Figure 19.- Comparison of slope of (jet) base pressure coefficient decay parameter for full-scale flight with wind-tunnel models and a semi-empirical estimate. $\lambda = 20°$.

	γ_j	Trailing-shock configuration	R	X
O Calculated from measured p_b	1.23	Conical	Approx. 2700	Approx. 0.65
□ Calculated from measured p_b	1.23	Plane	Approx. 2700	Approx. 0.65
◆ Reference 9	1.24	Plane	2300	1.0
⋈ Reference 9	1.23	Plane	Approx. 2700	Approx. 0.65

Apex of chevron represents data of reference 9 adjusted to conditions of calculated values (O,□).
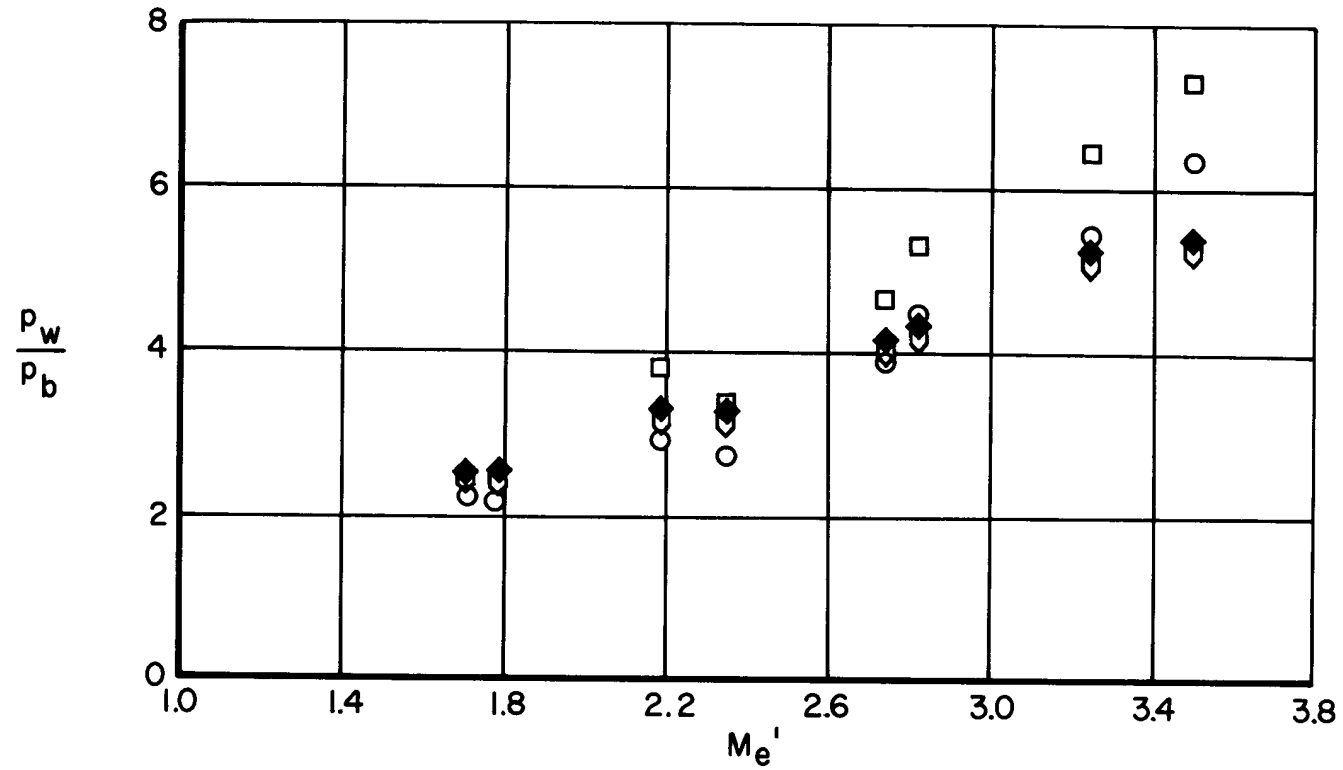

Figure 20.- Variation of trailing-shock pressure ratio with Mach number of external flow ahead of the shock.